Supporting Information for

Influence of Dithiolate Bridges on the Structures and Electrocatalytic Performance of Small Bite-Angle PNP-Chelated Diiron Complexes $Fe_2(\mu\text{-xdt})(CO)_4\{\kappa^2\text{-}(Ph_2P)_2NR\}$ Related to [FeFe]-Hydrogenases

Pei-Hua Zhao,[*,†] Meng-Yuan Hu,[†] Jian-Rong Li,[†] Zhong-Yi Ma,[†] Yan-Zhong Wang,[†] Jiao He,[‡] Yu-Long Li,[*,‡] and Xu-Feng Liu[§]

[†]School of Materials Science and Engineering, North University of China, Taiyuan 030051, P. R. China

[‡]College of Chemistry and Environmental Engineering, Sichuan University of Science & Engineering, Zigong 643000, P. R. China

[§]School of Materials and Chemical Engineering, Ningbo University of Technology, Ningbo 315211, P. R. China

*Corresponding author.

E-mail: zph2004@nuc.edu.cn (P.-H. Zhao); yu_longli@aliyun.com (Y.-L. Li).

Contents:

Part I: Selected crystallographic data for complexes 1a, 1b, 2a and 2d

Part II: Additional electrochemical studies of complexes 1b and 2b

Part III: IR and NMR (^{1}H, ^{31}P) spectra for complexes 1a–1e and 2a–2e

$Fe_2(\mu\text{-adt}^{NPh})(CO)_4\{\kappa^2\text{-}(Ph_2P)_2NCMe_3\}$ (**1a**) obtained from UV irradiation (method ii) in KBr disk.

$Fe_2(\mu\text{-adt}^{NPh})(CO)_4\{\kappa^2\text{-}(Ph_2P)_2N(CH_2)_3NMe_2\}$ (**1e**) obtained from UV irradiation (method ii) in KBr disk.

P30. **Figure S22.** ^{1}H NMR spectrum of $Fe_2(\mu\text{-adt}^{NPh})(CO)_4\{\kappa^2\text{-}(Ph_2P)_2N(CH_2)_3NMe_2\}$ (**1e**) in $CDCl_3$.

P31. **Figure S23.** $^{31}P\{^1H\}$ NMR spectrum of $Fe_2(\mu\text{-adt}^{NPh})(CO)_4\{\kappa^2\text{-}(Ph_2P)_2N(CH_2)_3NMe_2\}$ (**1e**) in $CDCl_3$.

P32. **Figure S24. (A)** FT-IR spectrum of $Fe_2(\mu\text{-edt})(CO)_4\{\kappa^2\text{-}(Ph_2P)_2NCMe_3\}$ (**2a**) obtained from oxidative decarbonylation (method i) in KBr disk; **(B)** FT-IR spectrum of $Fe_2(\mu\text{-edt})(CO)_4\{\kappa^2\text{-}(Ph_2P)_2NCMe_3\}$ (**2a**) obtained from UV irradiation (method ii) in KBr disk.

P33. **Figure S25.** ^{1}H NMR spectrum of $Fe_2(\mu\text{-edt})(CO)_4\{\kappa^2\text{-}(Ph_2P)_2NCMe_3\}$ (**2a**) in $CDCl_3$.

P34. **Figure S26.** $^{31}P\{^1H\}$ NMR spectrum of $Fe_2(\mu\text{-edt})(CO)_4\{\kappa^2\text{-}(Ph_2P)_2NCMe_3\}$ (**2a**) in $CDCl_3$.

P35. **Figure S27. (A)** FT-IR spectrum of $Fe_2(\mu\text{-edt})(CO)_4\{\kappa^2\text{-}(Ph_2P)_2NCH_2CHMe_2\}$ (**2b**) obtained from oxidative decarbonylation (method i) in KBr disk; **(B)** FT-IR spectrum of $Fe_2(\mu\text{-edt})(CO)_4\{\kappa^2\text{-}(Ph_2P)_2NCH_2CHMe_2\}$ (**2b**) obtained from UV irradiation (method ii) in KBr disk.

P36. **Figure S28.** ^{1}H NMR spectrum of $Fe_2(\mu\text{-edt})(CO)_4\{\kappa^2\text{-}(Ph_2P)_2NCH_2CHMe_2\}$ (**2b**) in $CDCl_3$.

P37. **Figure S29.** $^{31}P\{^1H\}$ NMR spectrum of $Fe_2(\mu\text{-edt})(CO)_4\{\kappa^2\text{-}(Ph_2P)_2NCH_2CHMe_2\}$ (**2b**) in $CDCl_3$.

P38. **Figure S30. (A)** FT-IR spectrum of $Fe_2(\mu\text{-edt})(CO)_4\{\kappa^2\text{-}(Ph_2P)_2N(CH_2)_3Me\}$ (**2c**) obtained from oxidative decarbonylation (method i) in KBr disk; **(B)** FT-IR spectrum of $Fe_2(\mu\text{-edt})(CO)_4\{\kappa^2\text{-}(Ph_2P)_2N(CH_2)_3Me\}$ (**2c**) obtained from UV irradiation (method ii) in KBr disk.

P39. **Figure S31.** ^{1}H NMR spectrum of $Fe_2(\mu\text{-edt})(CO)_4\{\kappa^2\text{-}(Ph_2P)_2N(CH_2)_3Me\}$ (**2c**) in $CDCl_3$.

P40. **Figure S32.** $^{31}P\{^1H\}$ NMR spectrum of $Fe_2(\mu\text{-edt})(CO)_4\{\kappa^2\text{-}(Ph_2P)_2N(CH_2)_3Me\}$ (**2c**) in $CDCl_3$.

P41. **Figure S33. (A)** FT-IR spectrum of $Fe_2(\mu\text{-edt})(CO)_4\{\kappa^2\text{-}(Ph_2P)_2N(CH_2)_2Si(OEt)_3\}$ (**2d**) obtained from oxidative decarbonylation (method i) in KBr disk; **(B)** FT-IR spectrum of $Fe_2(\mu\text{-edt})(CO)_4\{\kappa^2\text{-}(Ph_2P)_2N(CH_2)_2Si(OEt)_3\}$ (**2d**) obtained from UV irradiation (method ii) in KBr disk.

P42. **Figure S34.** ^{1}H NMR spectrum of $Fe_2(\mu\text{-edt})(CO)_4\{\kappa^2\text{-}(Ph_2P)_2N(CH_2)_3Si(OEt)_3\}$ (**2d**) in $CDCl_3$.

P43. **Figure S35.** $^{31}P\{^1H\}$ NMR spectrum of $Fe_2(\mu\text{-edt})(CO)_4\{\kappa^2\text{-}(Ph_2P)_2N(CH_2)_3Si(OEt)_3\}$ (**2d**) in $CDCl_3$.

P44. **Figure S36. (A)** FT-IR spectrum of $Fe_2(\mu\text{-edt})(CO)_4\{\kappa^2\text{-}(Ph_2P)_2N(CH_2)_3NMe_2\}$ (**2e**) obtained from oxidative decarbonylation (method i) in KBr disk; **(B)** FT-IR spectrum of $Fe_2(\mu\text{-edt})(CO)_4\{\kappa^2\text{-}(Ph_2P)_2N(CH_2)_3NMe_2\}$ (**2e**) obtained from UV irradiation (method ii) in KBr disk.

P45. **Figure S37.** ^1H NMR spectrum of $Fe_2(\mu\text{-edt})(CO)_4\{\kappa^2\text{-}(Ph_2P)_2N(CH_2)_3NMe_2\}$ (**2e**) in $CDCl_3$.

P46. **Figure S38.** $^{31}P\{^1H\}$ NMR spectrum of $Fe_2(\mu\text{-edt})(CO)_4\{\kappa^2\text{-}(Ph_2P)_2N(CH_2)_3NMe_2\}$ (**2e**) in $CDCl_3$.

Part I: Selected crystallographic data for complexes 1a, 1b, 2a and 2d

Table S1. Selected bond lengths and bond angles of complexes **1a**, **1b**, **2a** and **2d**

Complex	**1a**	**1b**	**2a**	**2d**
PNP configuration	Apical-basal	Dibasal	Apical-basal	Apical-basal
Bond distances (Å)				
Fe(1)-Fe(2)	2.5329(12)	2.5946(6)	2.5121(5)	2.5050(16)
Fe(2)-P(1)	2.1857(18)	2.2053(9)	2.1815(7)	2.183(2)
Fe(2)-P(2)	2.2060(16)	2.2058(9)	2.1908(7)	2.2229(19)
P(1)...P(2)	2.579(2)	2.5776(11)	2.5776(9)	2.596(2)
Fe(2)-C(4)	1.741(7)	1.760(3)	1.746(3)	1.753(8)
Fe(1)...C(4)	3.105	4.183	3.256	3.262
Bond angles (°)				
P(1)-Fe(2)-Fe(1)	156.99(6)	111.04(3)	165.29(3)	155.08(7)
P(2)-Fe(2)-Fe(1)	124.80(6)	115.49(3)	115.73(2)	119.32(7)
P(1)-Fe(2)-P(2)	71.92(6)	71.51(3)	72.25(3)	72.20(7)
P(1)-N-P(2)	96.4(3)	97.47(13)	96.90(10)	99.2(3)
Fe(1)-Fe(2)-C(4)	91.3(3)	147.10(10)	98.13(8)	98.5(3)
C(5)-N-C(6)	113.6(5)	113.9(3)	-	-
C(6)-N-C(7)	122.9(5)	119.8(3)	-	-
C(5)-N-C(7)	123.2(5)	121.9(3)	-	-

Table S2. Details of crystallographic data and structure refinement for **1a**, **1b**, **2a** and **2d**

Complex	**1a**	**1b**	**2a**	**2d**
CCDC number	1865617	1865618	1865619	1865625
Empirical formula	$C_{40}H_{38}Fe_2N_2O_4P_2S_2$	$C_{40}H_{38}Fe_2N_2O_4P_2S_2\cdot CH_2Cl_2$	$C_{34}H_{33}Fe_2NO_4P_2S_2$	$C_{39}H_{45}Fe_2NO_7P_2S_2Si$
Formula weight	848.48	933.41	757.37	905.61
Temperature (K)	296(2)	296(2)	296(2)	296(2)
Wavelength (Å)	0.71073	0.71073	0.71073	0.71073
Crystal system	triclinic	triclinic	monoclinic	orthorhombic
Space group	P-1	P-1	$P2_1/n$	Pbca
a (Å)	10.5181(7)	10.4095(10)	10.8939(9)	17.476(5)
b (Å)	10.9702(8)	11.6260(10)	14.7675(10)	19.435(5)
c (Å)	19.7269(14)	18.6195(17)	21.5753(16)	25.393(7)
α (°)	74.368(2)	80.837(2)	90	90
β (°)	81.839(2)	88.750(3)	102.095(2)	90
γ (°)	64.218(2)	73.220(3)	90	90
V (Å^3)	1973.0(2)	2129.2(3)	3393.9(4)	8624(4)
Z	2	2	4	8
D_{calc} (g cm^{-3})	1.428	1.456	1.482	1.395
μ (mm^{-1})	0.965	1.023	1.111	0.918
F(000)	876.0	960.0	1560.0	3760.0
Crystal size (mm)	0.30×0.20×0.16	0.38×0.22×0.18	0.26×0.22×0.16	0.32×0.28×0.22
θ_{min}, θ_{max} (°)	4.282, 50.888	4.434, 50.864	4.630, 50.142	4.192, 50.270
Reflections collected/unique	36440/7239	53767/7816	71129/6011	160466/7695
R_{int}	0.0559	0.0506	0.0553	0.0993
hkl Range	$-12 \leq h \leq 12$ $-13 \leq k \leq 13$ $-23 \leq l \leq 23$	$-12 \leq h \leq 12$ $-13 \leq k \leq 14$ $-22 \leq l \leq 22$	$-12 \leq h \leq 12$ $-17 \leq k \leq 17$ $-25 \leq l \leq 25$	$-20 \leq h \leq 20$ $-22 \leq k \leq 23$ $-30 \leq l \leq 30$
Completeness to θ_{max} (%)	99.4	99.5	99.9	99.7
Data/restraints/parameters	7239/26/472	7816/0/508	6011/0/409	7695/79/490
Goodness-of-fit (GOF) on F^2	1.065	1.169	1.117	1.152
R_1/wR_2 [$I > 2\sigma(I)$]	0.0662/0.1849	0.0405/0.1274	0.0319/0.0812	0.0946/0.2446
R_1/wR_2 (all data)	0.1052/0.2148	0.0511/0.1446	0.0492/0.0948	0.1304/0.2742
Largest difference peak/ hole (e A^{-3})	1.25/-0.80	0.78/-0.84	0.42/-0.48	0.96/-0.89

Part II: Additional electrochemical studies of complexes 1b and 2b

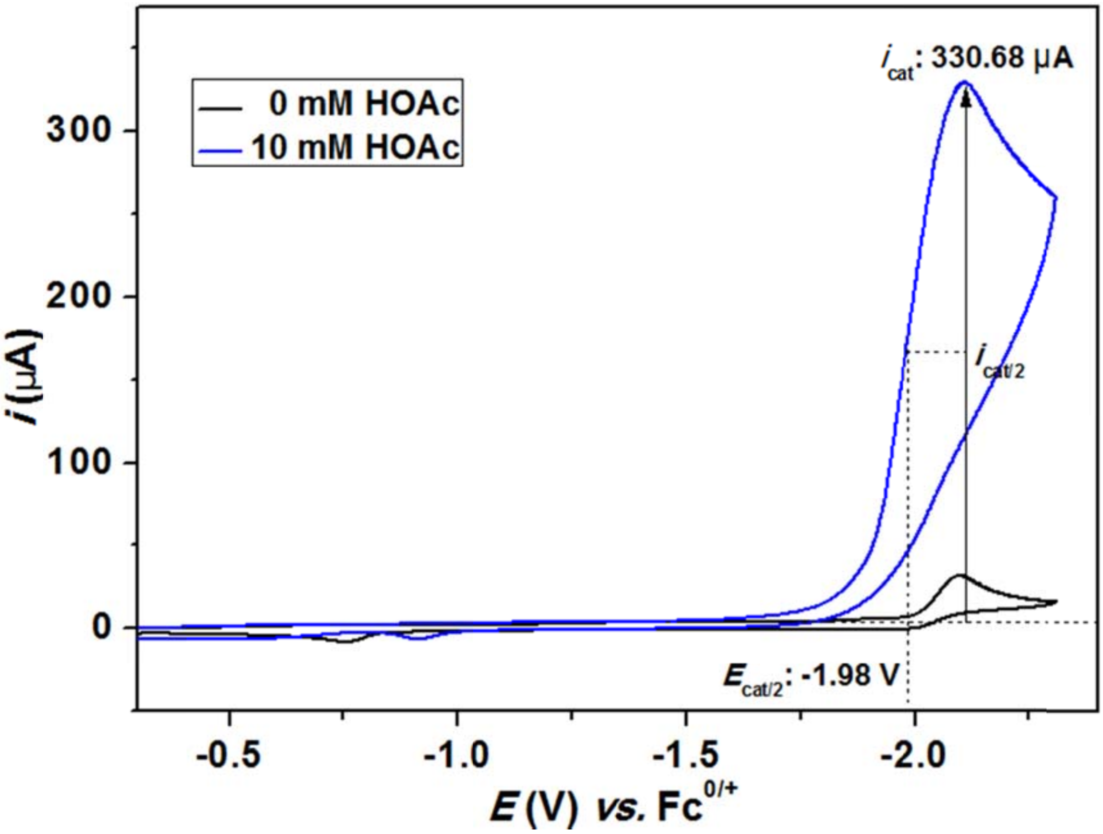

Figure S1. Cyclic voltammograms of **1b** (1.0 mM) with HOAc (0, 10 mM) in 0.1 M n-Bu_4NPF_6/ MeCN solution at a scan rate of 0.1 V s^{-1}.

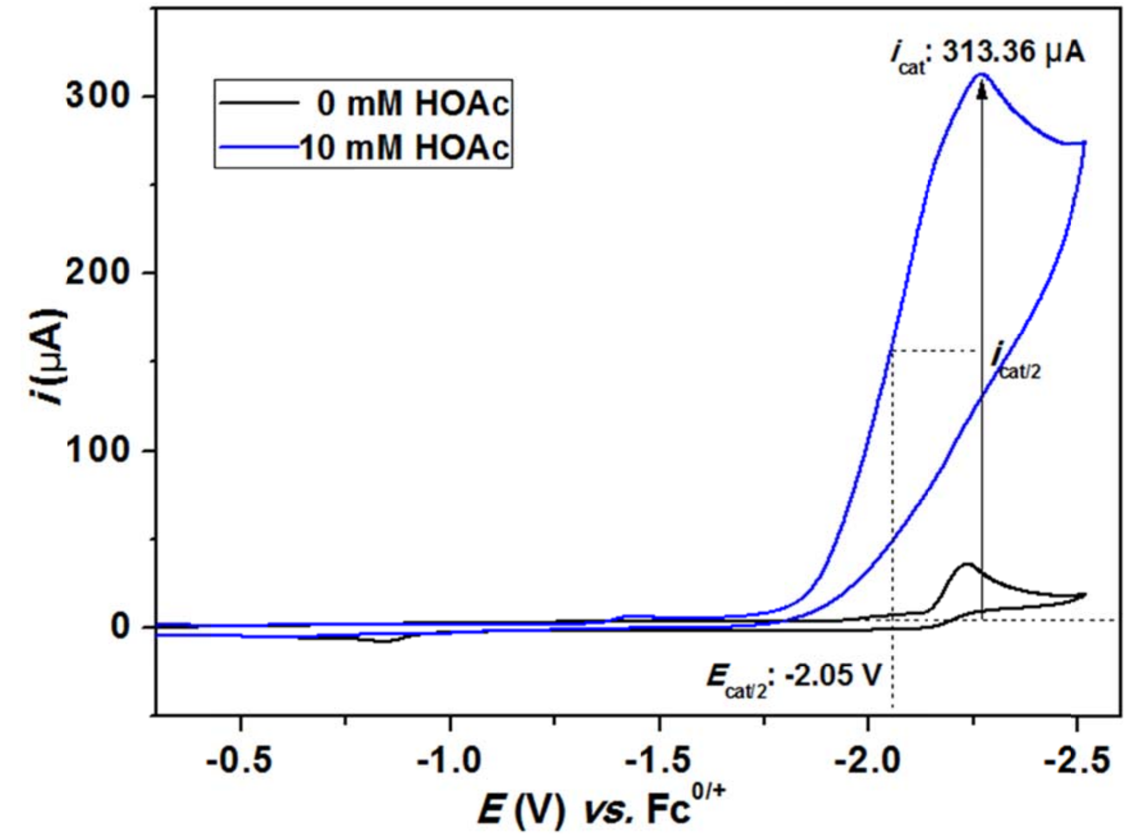

Figure S2. Cyclic voltammograms of **2b** (1.0 mM) with HOAc (0, 10 mM) in 0.1 M n-Bu_4NPF_6/ MeCN solution at a scan rate of 0.1 V s^{-1}.

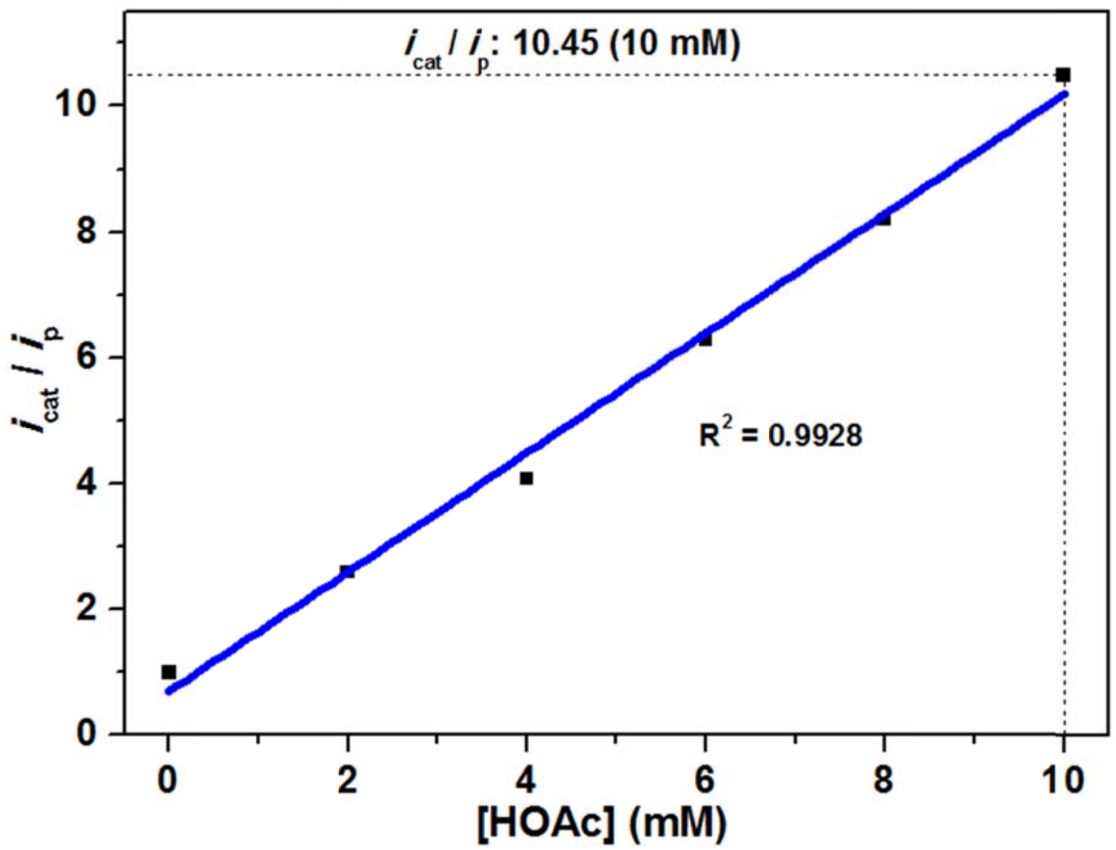

Figure S3. Plots of i_{cat}/i_p versus [HOAc] (mM) for **1b** (1.0 mM) in 0.1 M n-Bu_4NPF_6/ MeCN solution at a scan rate of 0.1 V s^{-1}.

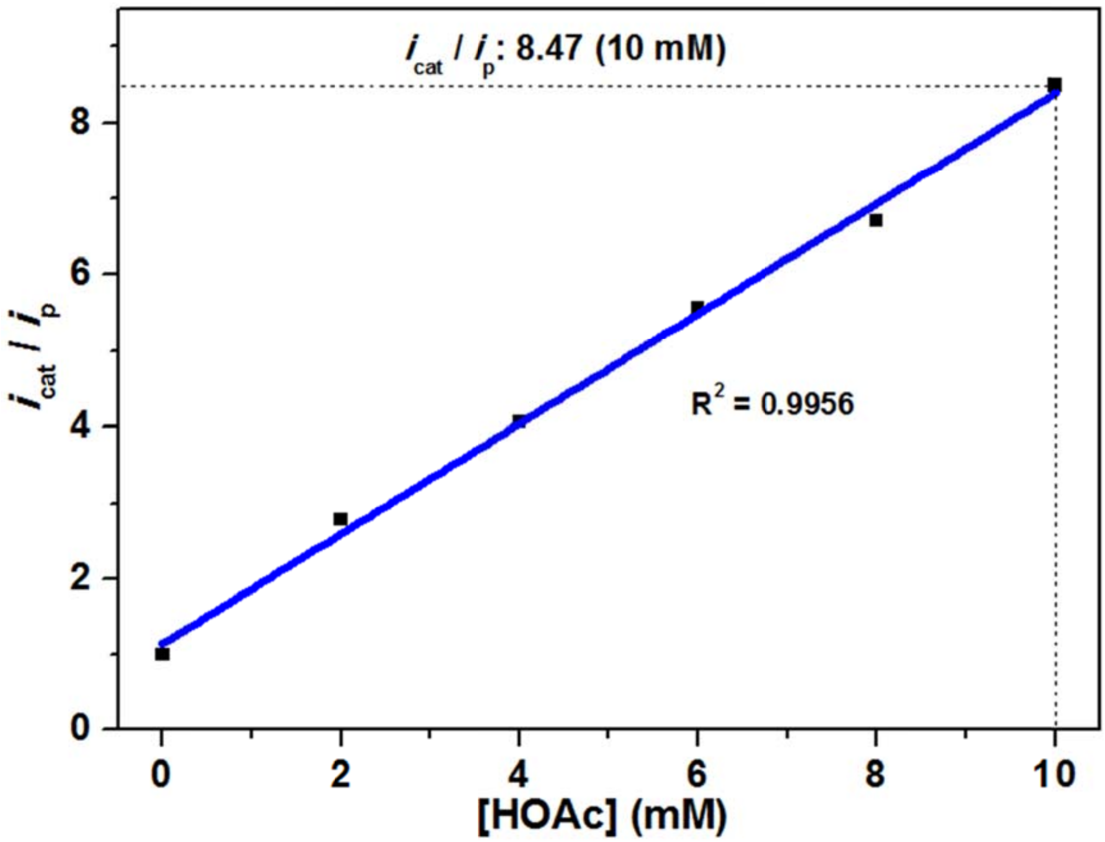

Figure S4. Plots of i_{cat}/i_p versus [HOAc] (mM) for **2b** (1.0 mM) in 0.1 M ***n***-Bu_4NPF_6/MeCN solution at a scan rate of 0.1 V s^{-1}.

Table S3. The relevant electrochemical data for complexes **1a**, **1c–1e** and **2a**, **2c–2e**

Complex	E_{pc} (V)	$E_{cat/2}$ (V)	Overpotential (V)	i_{cat}/i_p	*k* (TOF) (s^{-1})
1a	-2.12	-2.03	0.65	15.87	48.86
2a	-2.16	-2.10	0.72	11.67	26.42
1c	-2.11	-1.99	0.61	10.18	20.10
2c	-2.24	-2.06	0.68	7.80	11.80
1d	-2.21	-2.01	0.63	4.08	3.23
2d	-2.22	-2.13	0.75	2.26	0.99
1e	-2.11	-2.05	0.67	11.34	24.95
2e	-2.15	-2.15	0.77	7.93	12.20

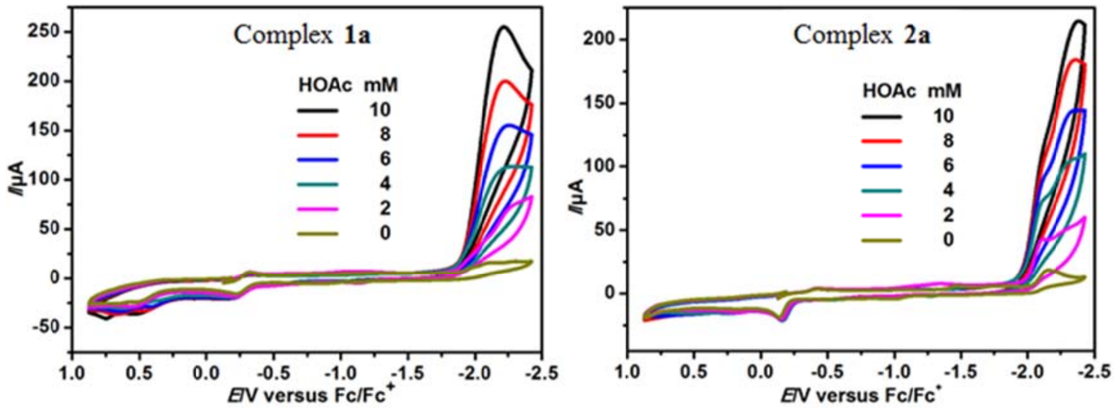

Figure S5. Cyclic voltammograms of **1a** (1.0 mM, left) and **2a** (1.0 mM, right) with HOAc (0, 2, 4, 6, 8, 10 mM) in 0.1 M n-Bu_4NPF_6/MeCN solution at a scan rate of 0.1 V s^{-1}. All potentials are versus ferrocene/ferrocenium ($Fc^{0/+}$) couple.

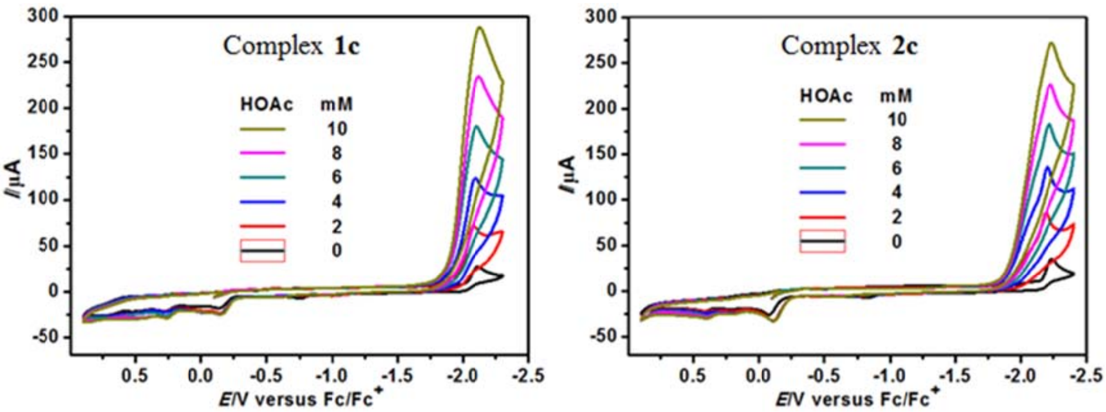

Figure S6. Cyclic voltammograms of **1c** (1.0 mM, left) and **2c** (1.0 mM, right) with HOAc (0, 2, 4, 6, 8, 10 mM) in 0.1 M n-Bu_4NPF_6/MeCN solution at a scan rate of 0.1 V s^{-1}. All potentials are versus ferrocene/ferrocenium ($Fc^{0/+}$) couple.

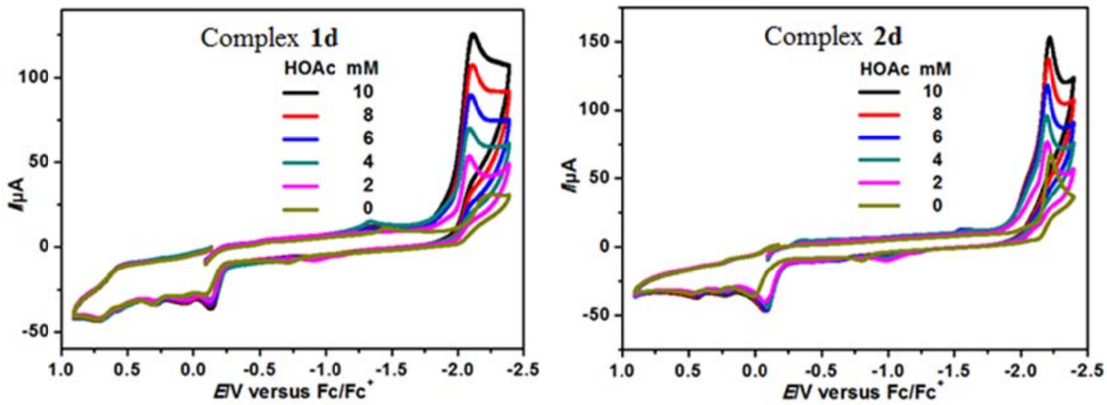

Figure S7. Cyclic voltammograms of **1d** (1.0 mM, left) and **2d** (1.0 mM, right) with HOAc (0, 2, 4, 6, 8, 10 mM) in 0.1 M n-Bu_4NPF_6/MeCN solution at a scan rate of 0.1 V s^{-1}. All potentials are versus ferrocene/ferrocenium ($Fc^{0/+}$) couple.

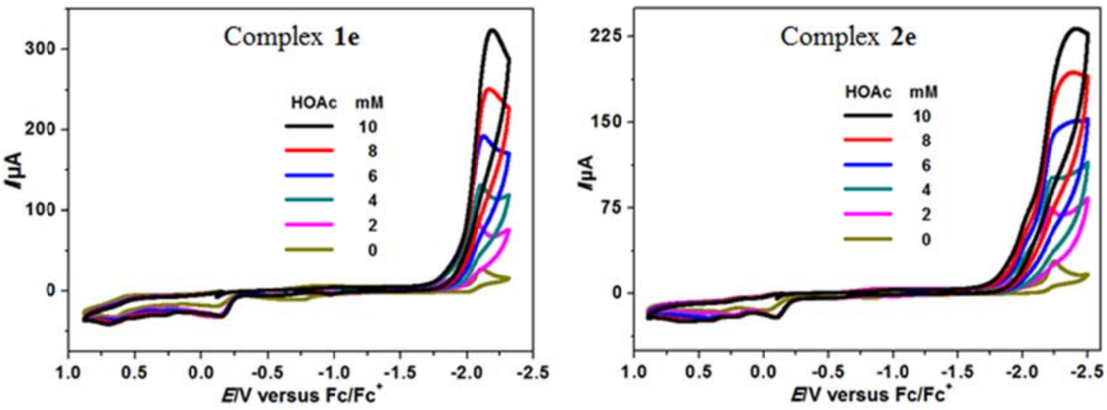

Figure S8. Cyclic voltammograms of **1e** (1.0 mM, left) and **2e** (1.0 mM, right) with HOAc (0, 2, 4, 6, 8, 10 mM) in 0.1 M n-Bu_4NPF_6/MeCN solution at a scan rate of 0.1 V s^{-1}. All potentials are versus ferrocene/ferrocenium ($Fc^{0/+}$) couple.

Part III: The IR and NMR (^{1}H, ^{31}P) spectra for complexes 1a–1e and 2a–2e

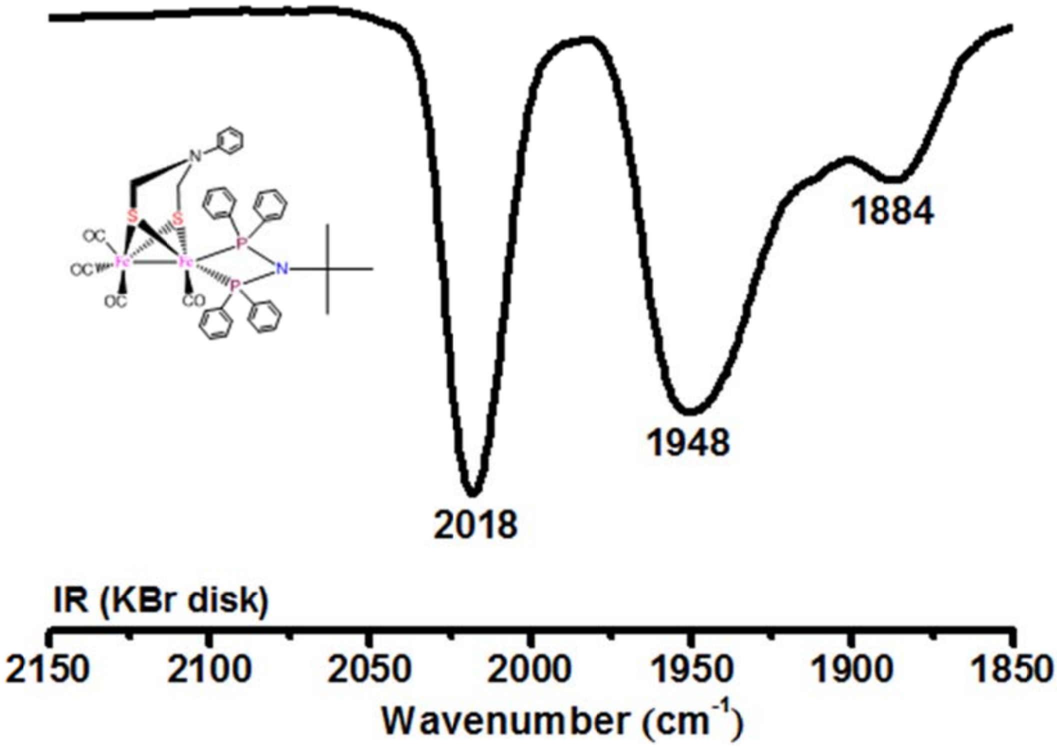

Figure S9(A). FT-IR spectrum of $Fe_2(\mu\text{-adt}^{NPh})(CO)_4\{\kappa^2\text{-}(Ph_2P)_2NCMe_3\}$ (**1a**) obtained from oxidative decarbonylation (method i)in KBr disk.

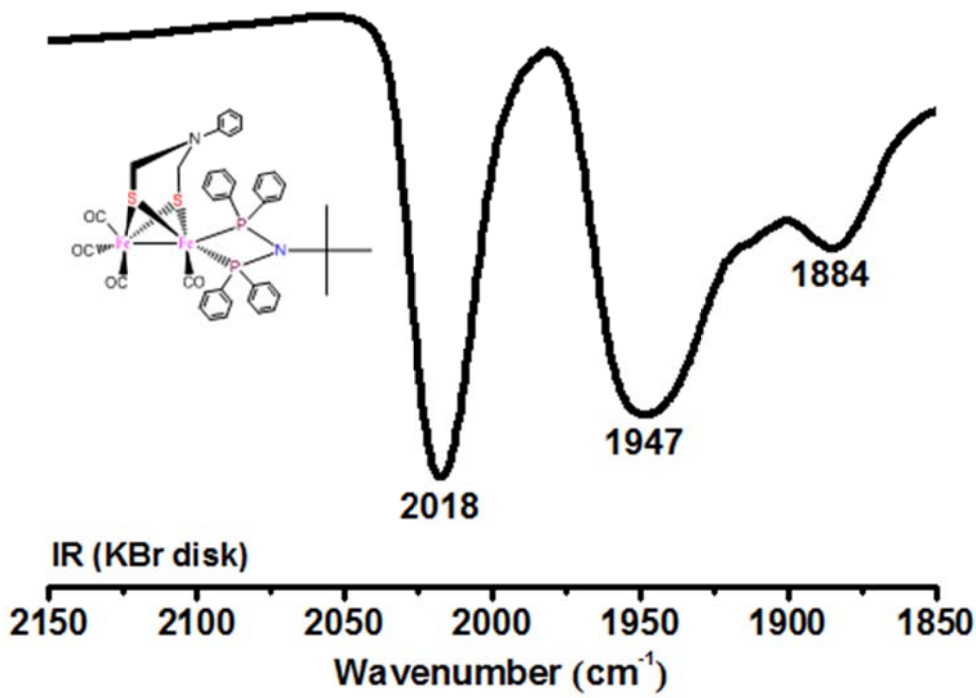

Figure S9(B). FT-IR spectrum of $Fe_2(\mu\text{-adt}^{NPh})(CO)_4\{\kappa^2\text{-}(Ph_2P)_2NCMe_3\}$ (**1a**) obtained from UV irradiation (method ii) in KBr disk.

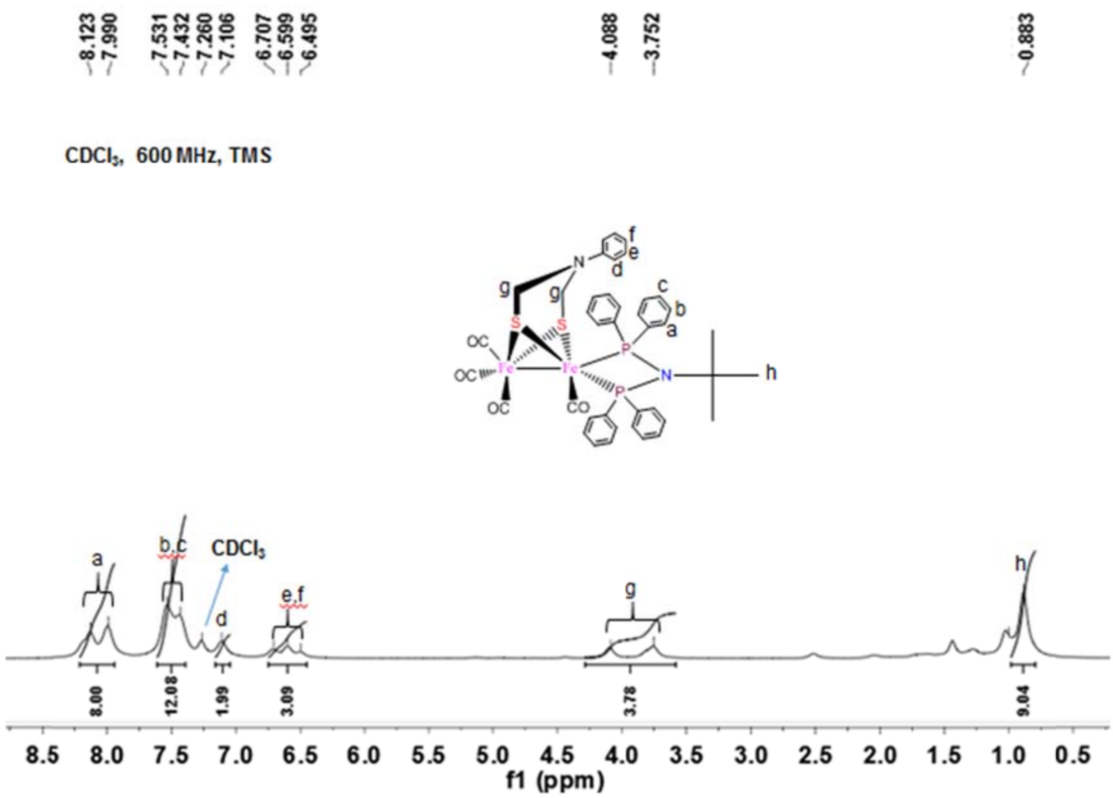

Figure S10. ^{1}H NMR spectrum of $Fe_2(\mu\text{-}adt^{NPh})(CO)_4\{\kappa^2\text{-}(Ph_2P)_2NCMe_3\}$ (**1a**) in $CDCl_3$.

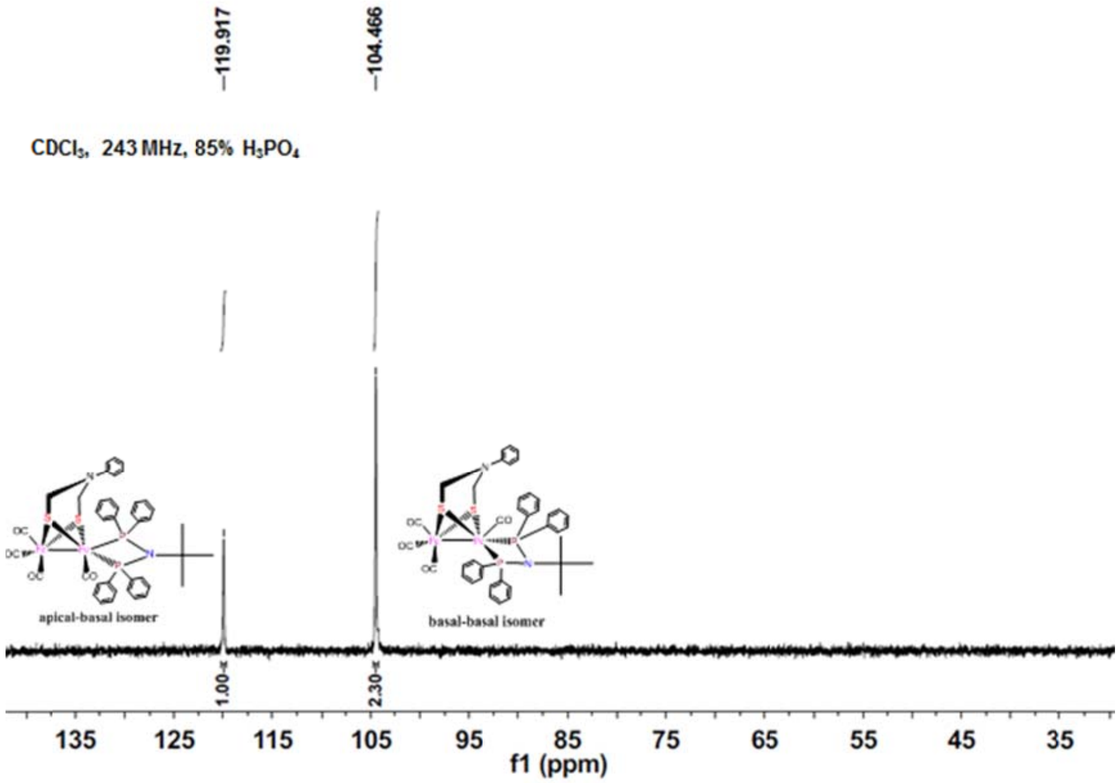

Figure S11. $^{31}P\{^{1}H\}$ NMR spectrum of $Fe_2(\mu\text{-adt}^{NPh})(CO)_4\{\kappa^2\text{-}(Ph_2P)_2NCMe_3\}$ (**1a**) in $CDCl_3$.

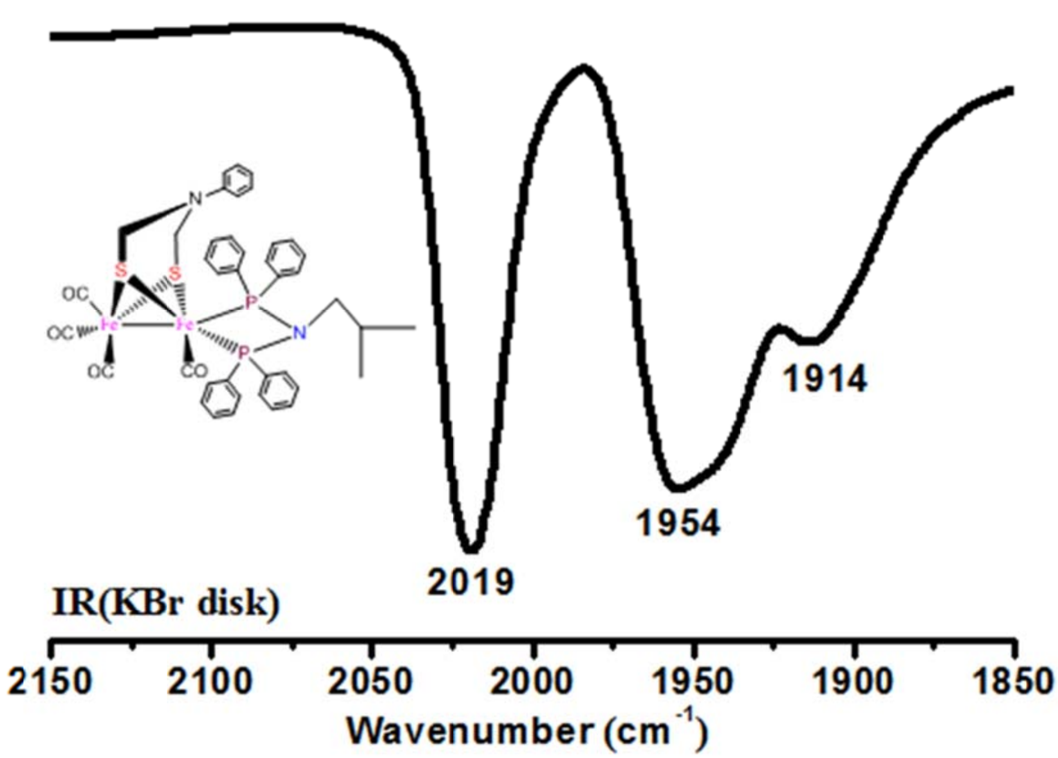

Figure S12(A). FT-IR spectrum of $Fe_2(\mu\text{-adt}^{NPh})(CO)_4\{\kappa^2\text{-}(Ph_2P)_2NCH_2CHMe_2\}$ (**1b**) obtained from oxidative decarbonylation (method i) in KBr disk.

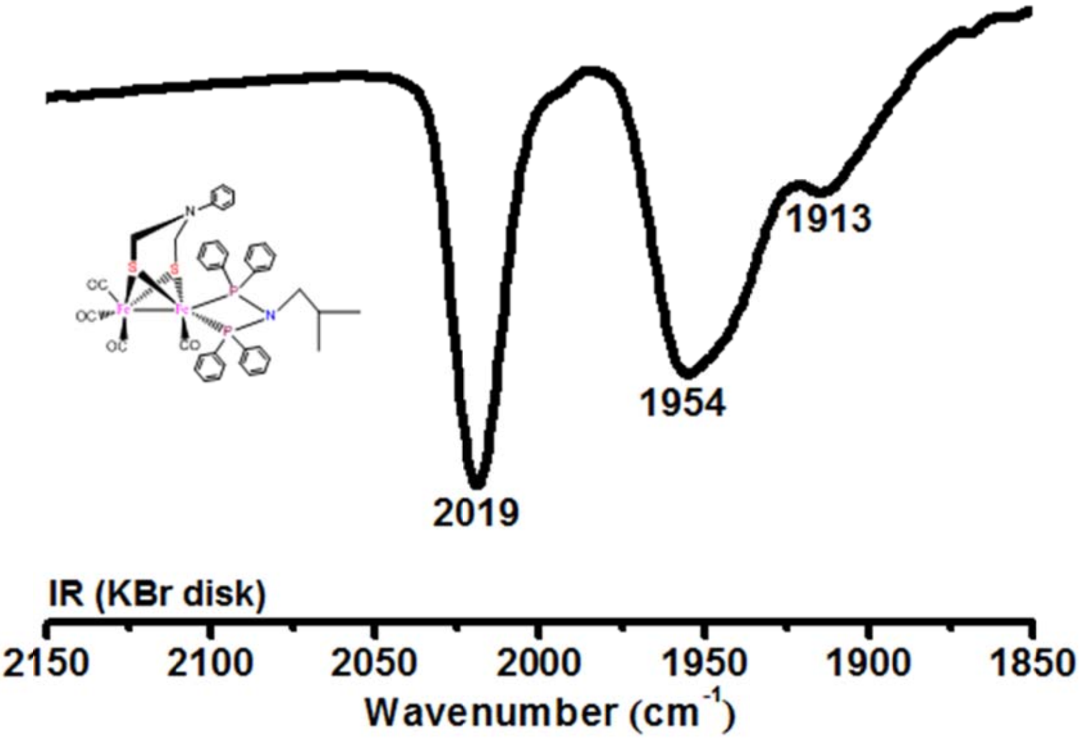

Figure S12(B). FT-IR spectrum of $Fe_2(\mu\text{-adt}^{NPh})(CO)_4\{\kappa^2\text{-}(Ph_2P)_2NCH_2CHMe_2\}$ (**1b**) obtained from UV irradiation (method ii) in KBr disk.

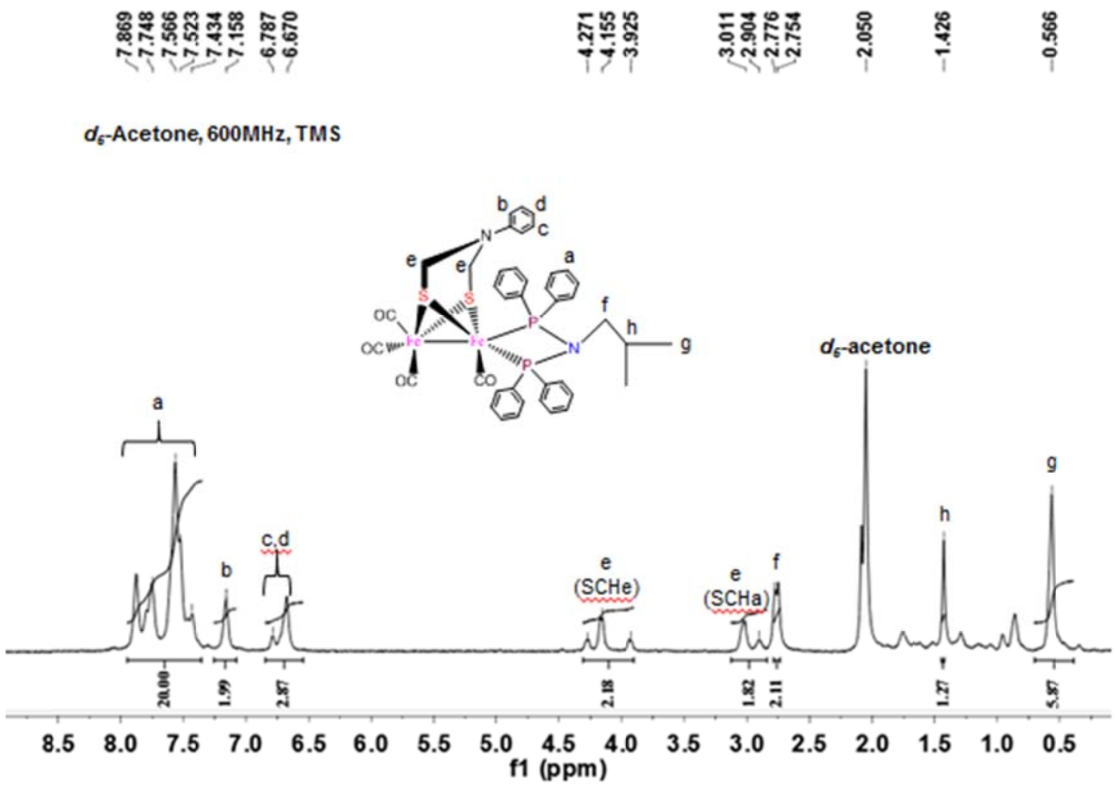

Figure S13. ^{1}H NMR spectrum of $Fe_2(\mu\text{-adt}^{NPh})(CO)_4\{\kappa^2\text{-}(Ph_2P)_2NCH_2CHMe_2\}$ (**1b**) in *d*$_6$-acetone.

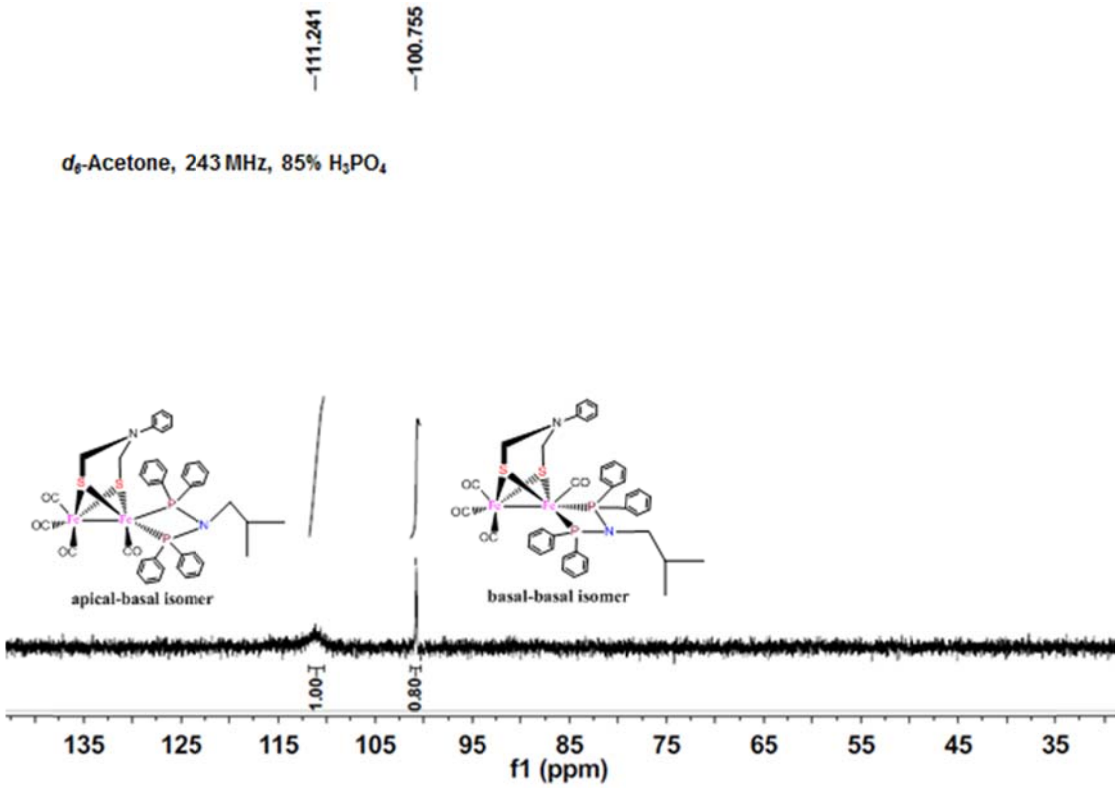

Figure S14. $^{31}P\{^{1}H\}$ NMR spectrum of $Fe_2(\mu\text{-adt}^{NPh})(CO)_4\{\kappa^2\text{-}(Ph_2P)_2NCH_2CHMe_2\}$ (**1b**) in d_6-acetone.

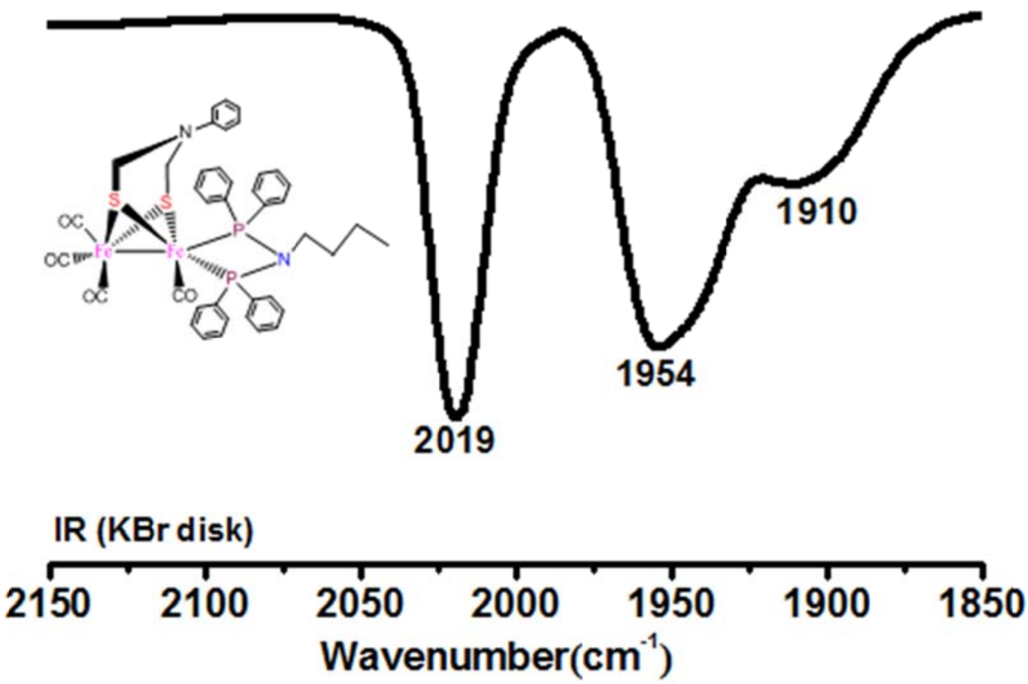

Figure S15(A). FT-IR spectrum of $Fe_2(\mu\text{-adt}^{NPh})(CO)_4\{\kappa^2\text{-}(Ph_2P)_2N(CH_2)_3Me\}$ (**1c**) obtained from oxidative decarbonylation (method i) in KBr disk.

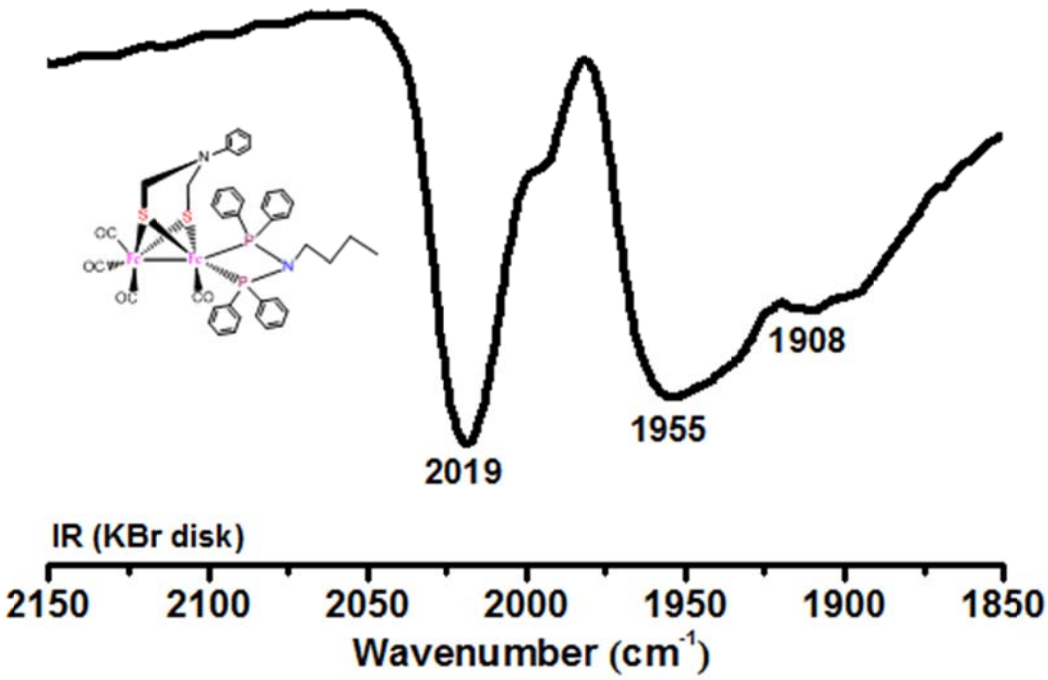

Figure S15(B). FT-IR spectrum of $Fe_2(\mu\text{-adt}^{NPh})(CO)_4\{\kappa^2\text{-}(Ph_2P)_2N(CH_2)_3Me\}$ (**1c**) obtained from UV irradiation (method ii) in KBr disk.

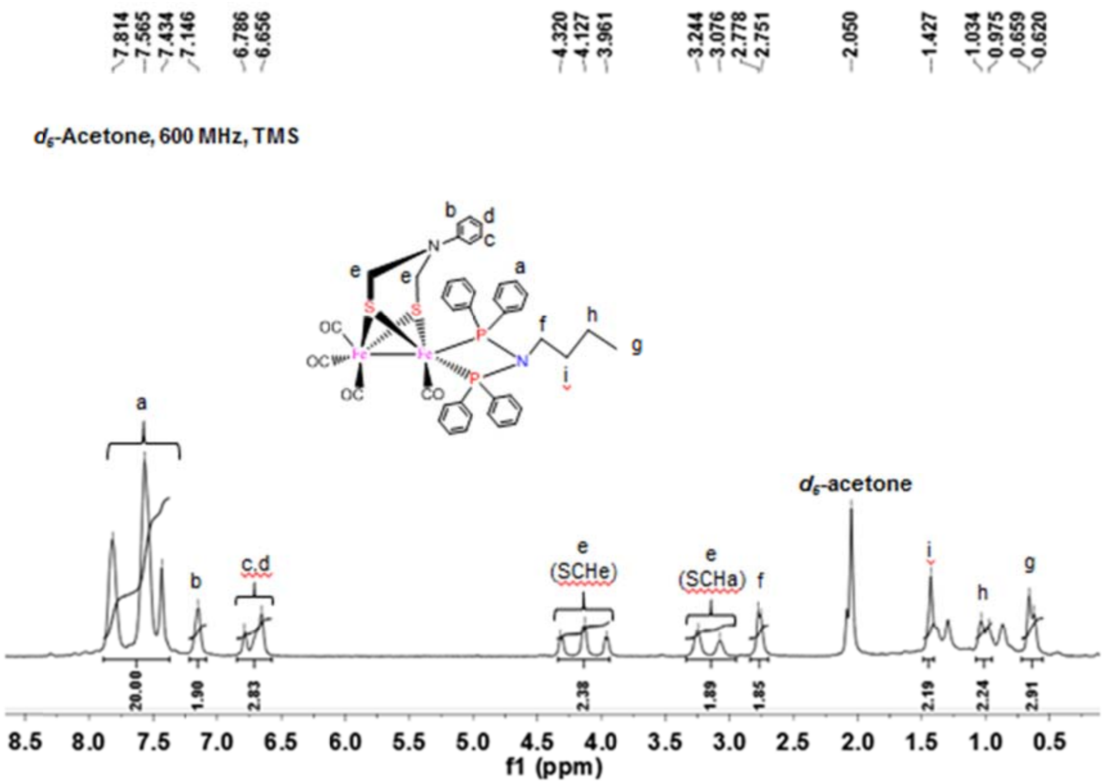

Figure S16. ^{1}H NMR spectrum of $Fe_2(\mu\text{-adt}^{NPh})(CO)_4\{\kappa^2\text{-}(Ph_2P)_2N(CH_2)_3Me\}$ (**1c**) in d_6-acetone.

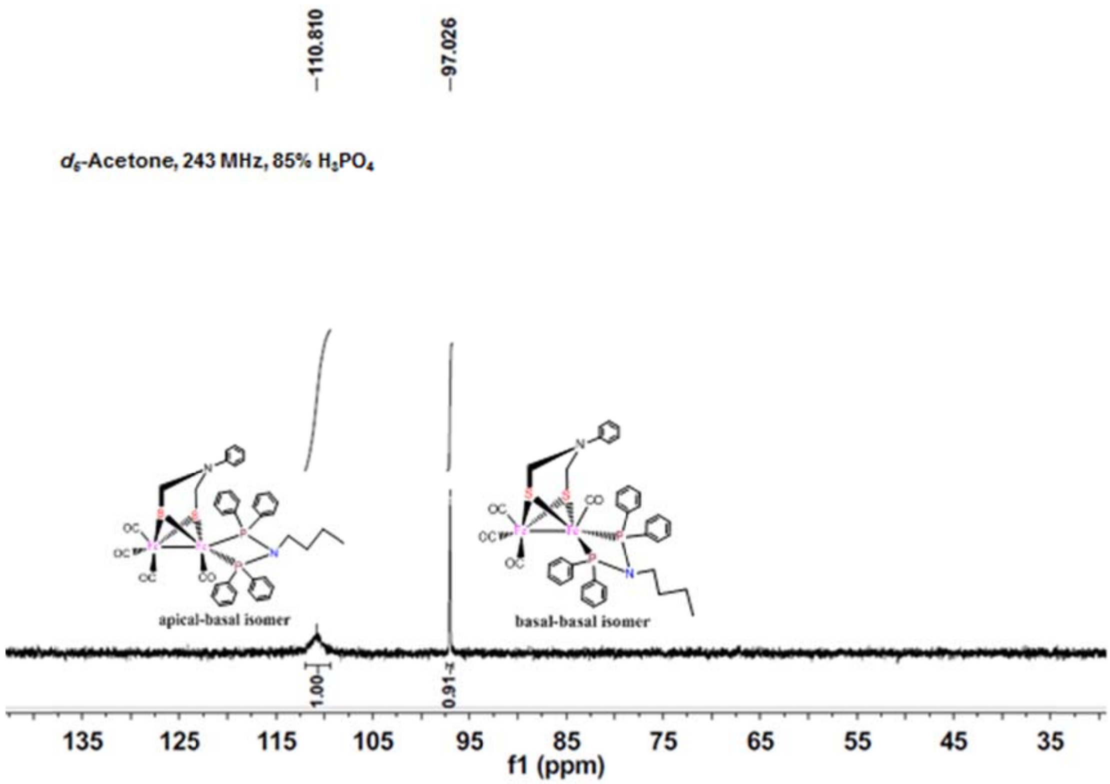

Figure S17. $^{31}P\{^{1}H\}$ NMR spectrum of $Fe_2(\mu\text{-adt}^{NPh})(CO)_4\{\kappa^2\text{-}(Ph_2P)_2N(CH_2)_3Me\}$ (**1c**) in d_6-acetone.

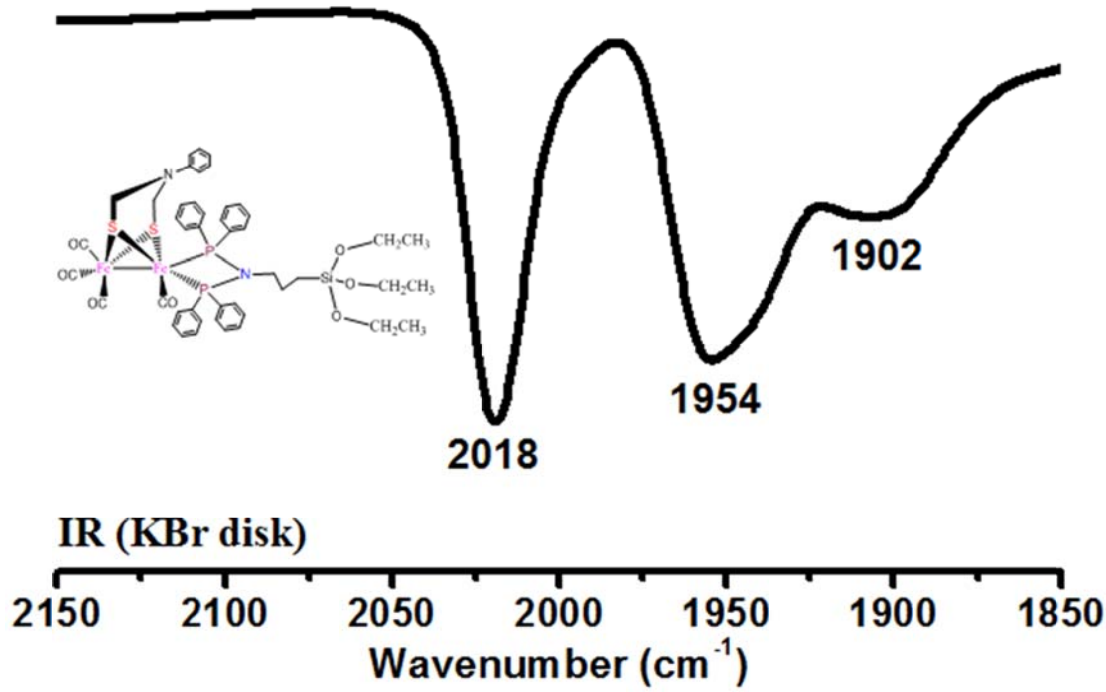

Figure S18(A). FT-IR spectrum of Fe_2(μ-adt^{NPh})$(CO)_4${κ^2-$(Ph_2P)_2N(CH_2)_3Si(OEt)_3$} (**1d**) obtained from oxidative decarbonylation (method i) in KBr disk.

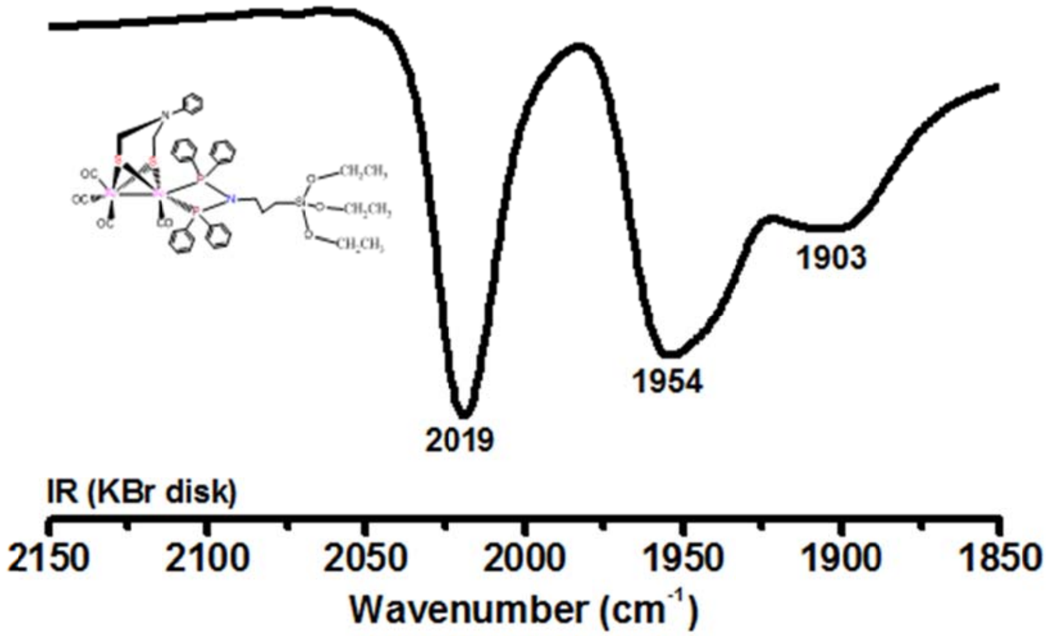

Figure S18(B). FT-IR spectrum of Fe_2(μ-adt^{NPh})$(CO)_4${κ^2-$(Ph_2P)_2N(CH_2)_3Si(OEt)_3$} (**1d**) obtained from UV irradiation (method ii) in KBr disk.

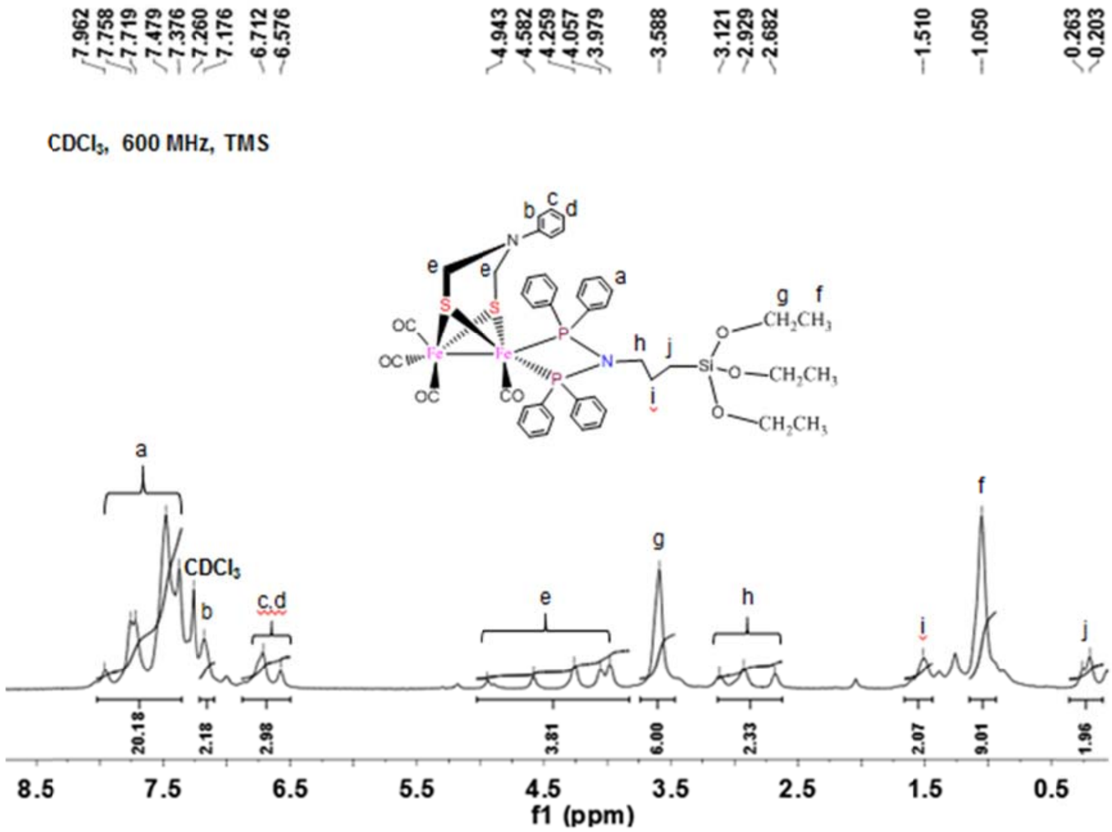

Figure S19. ^{1}H NMR spectrum of $Fe_2(\mu\text{-adt}^{NPh})(CO)_4\{\kappa^2\text{-}(Ph_2P)_2N(CH_2)_3Si(OEt)_3\}$ (**1d**) in $CDCl_3$.

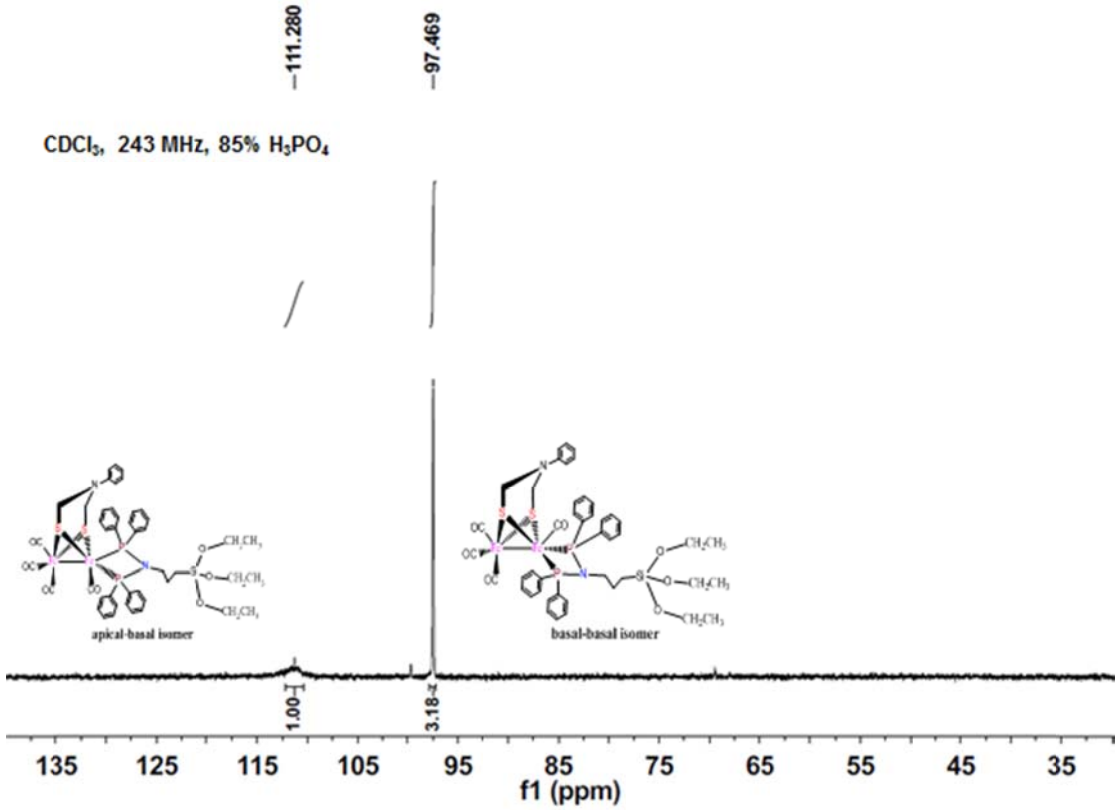

Figure S20. $^{31}P\{^{1}H\}$ NMR spectrum of $Fe_2(\mu\text{-adt}^{NPh})(CO)_4\{\kappa^2\text{-}(Ph_2P)_2N(CH_2)_3Si(OEt)_3\}$ (**1d**) in $CDCl_3$.

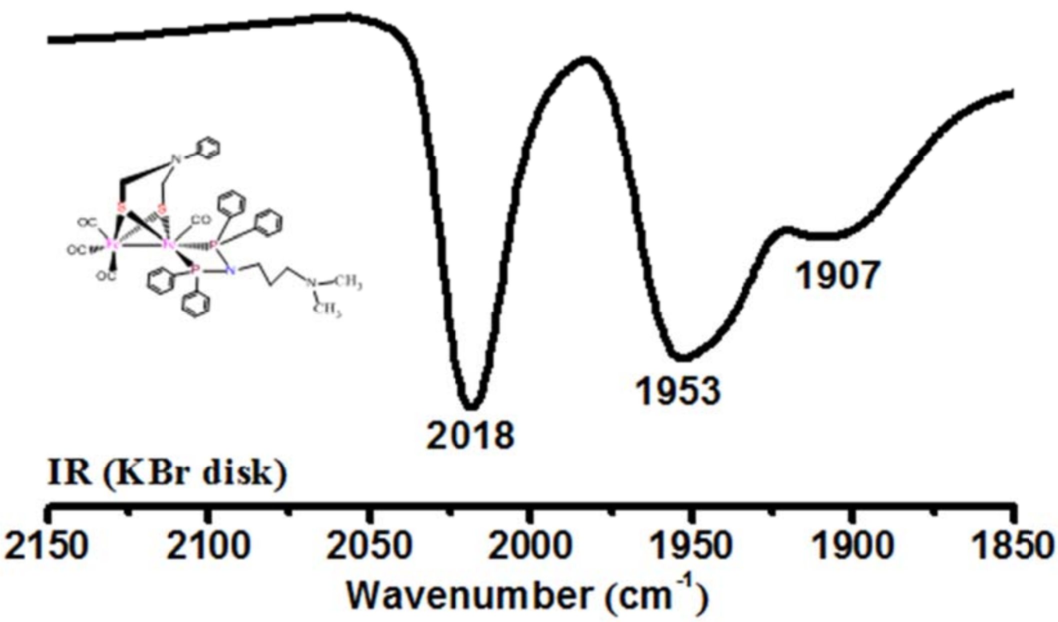

Figure S21(A). FT-IR spectrum of $Fe_2(\mu\text{-adt}^{NPh})(CO)_4\{\kappa^2\text{-}(Ph_2P)_2N(CH_2)_3NMe_2\}$ (**1e**) obtained from oxidative decarbonylation (method i) in KBr disk.

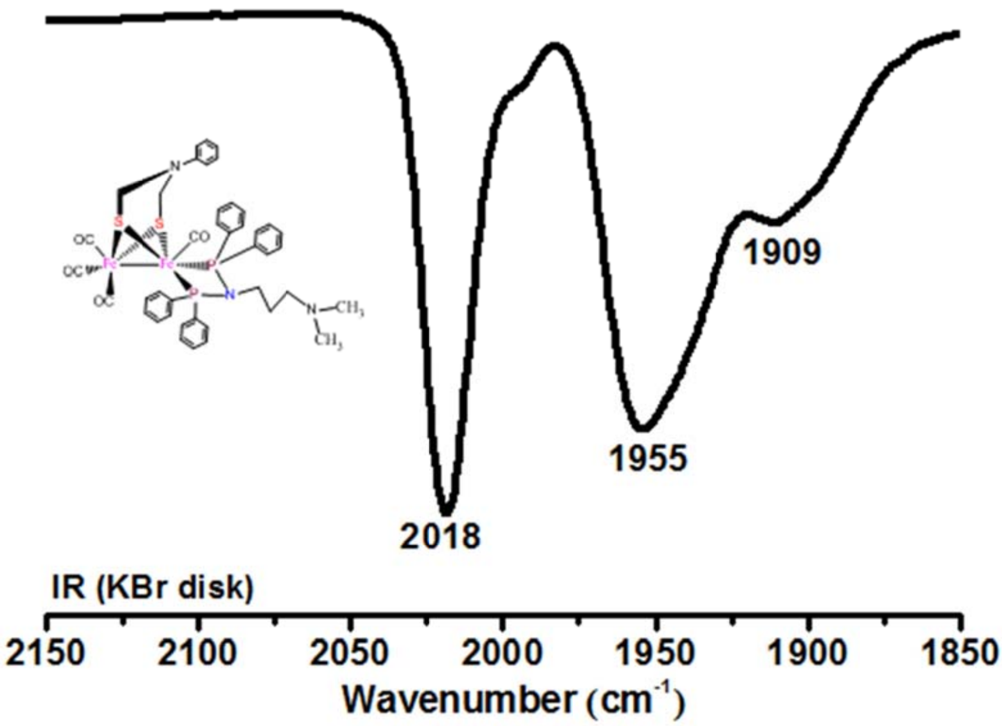

Figure S21(B). FT-IR spectrum of $Fe_2(\mu\text{-adt}^{NPh})(CO)_4\{\kappa^2\text{-}(Ph_2P)_2N(CH_2)_3NMe_2\}$ (**1e**) obtained from UV irradiation (method ii) in KBr disk.

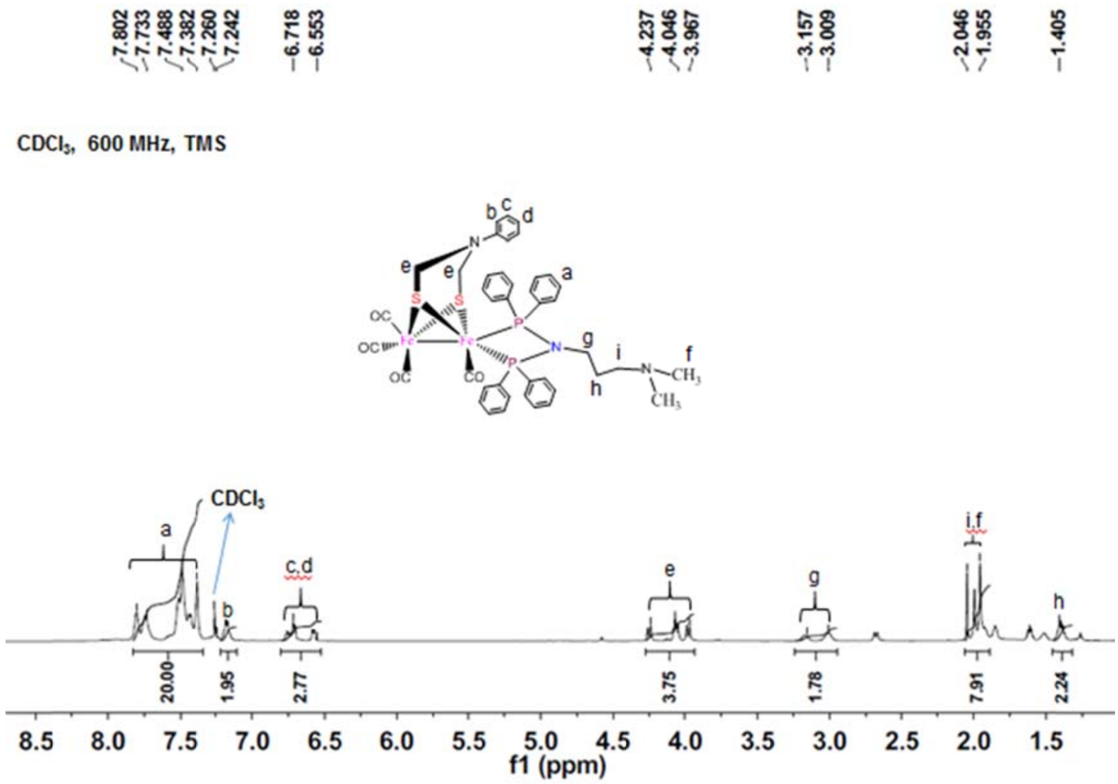

Figure S22. ^{1}H NMR spectrum of $Fe_2(\mu\text{-adt}^{NPh})(CO)_4\{\kappa^2\text{-}(Ph_2P)_2N(CH_2)_3NMe_2\}$ (**1e**) in $CDCl_3$.

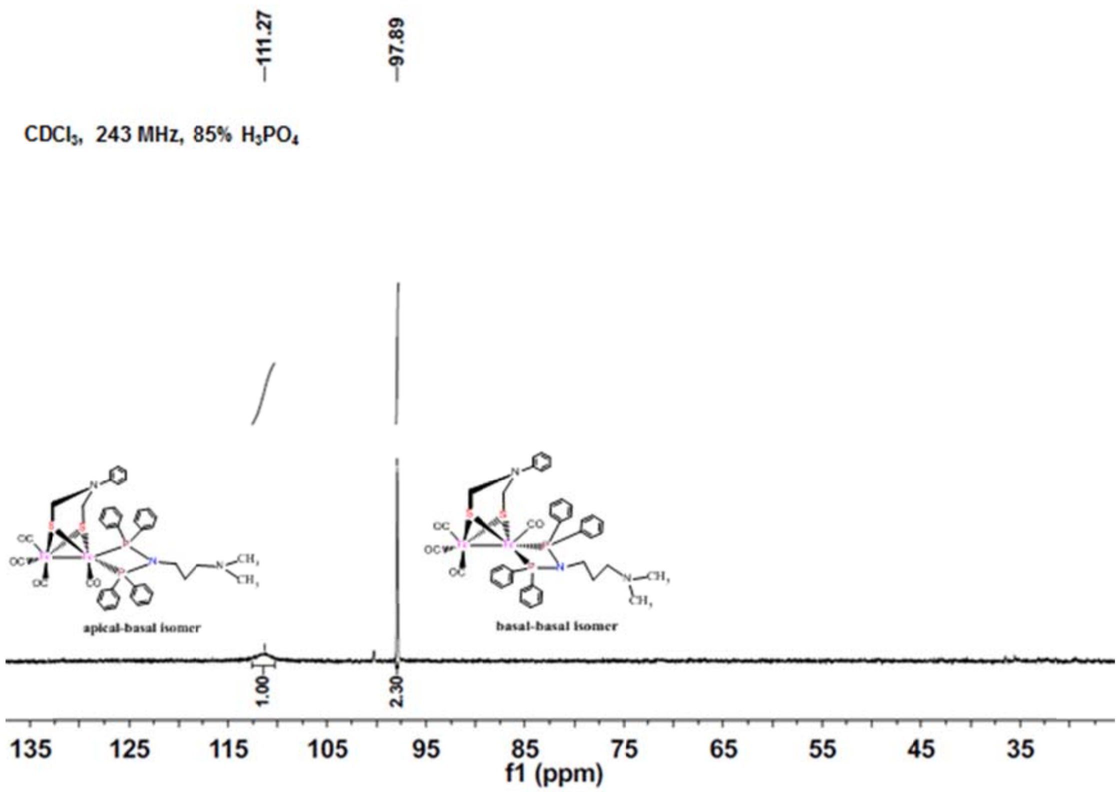

Figure S23. $^{31}P\{^{1}H\}$ NMR spectrum of $Fe_2(\mu\text{-adt}^{NPh})(CO)_4\{\kappa^2\text{-}(Ph_2P)_2N(CH_2)_3NMe_2\}$ (**1e**) in $CDCl_3$.

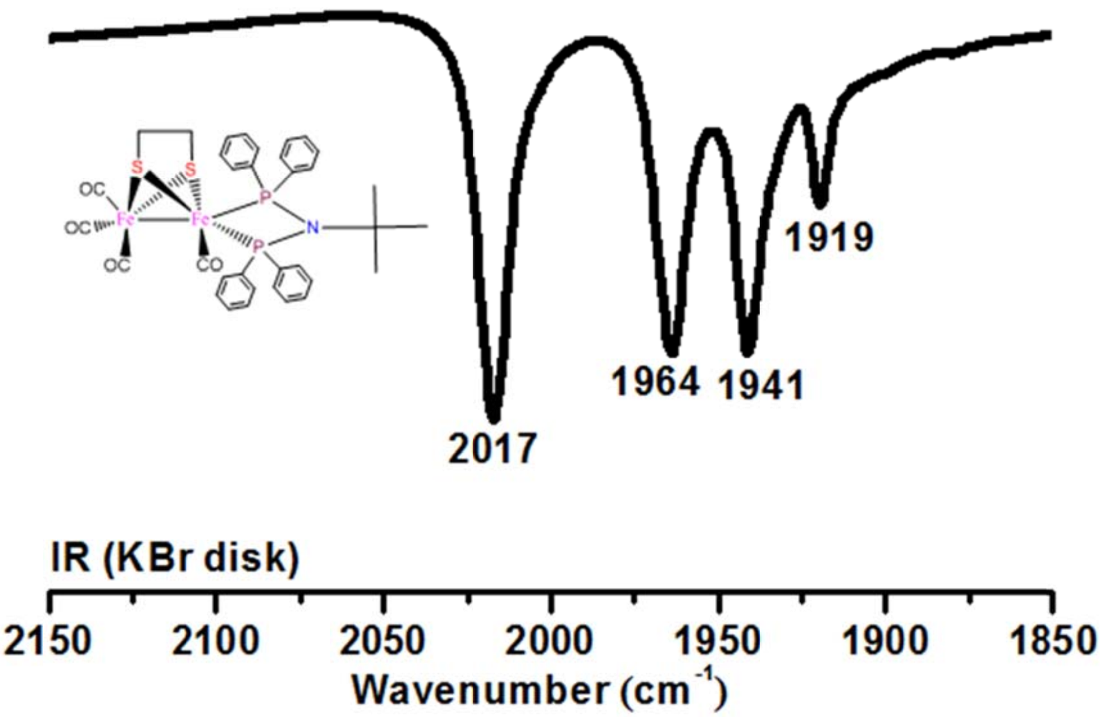

Figure S24(A). FT-IR spectrum of Fe_2(μ-edt)$(CO)_4${κ^2-$(Ph_2P)_2NCMe_3$} (**2a**) obtained from oxidative decarbonylation (method i) in KBr disk.

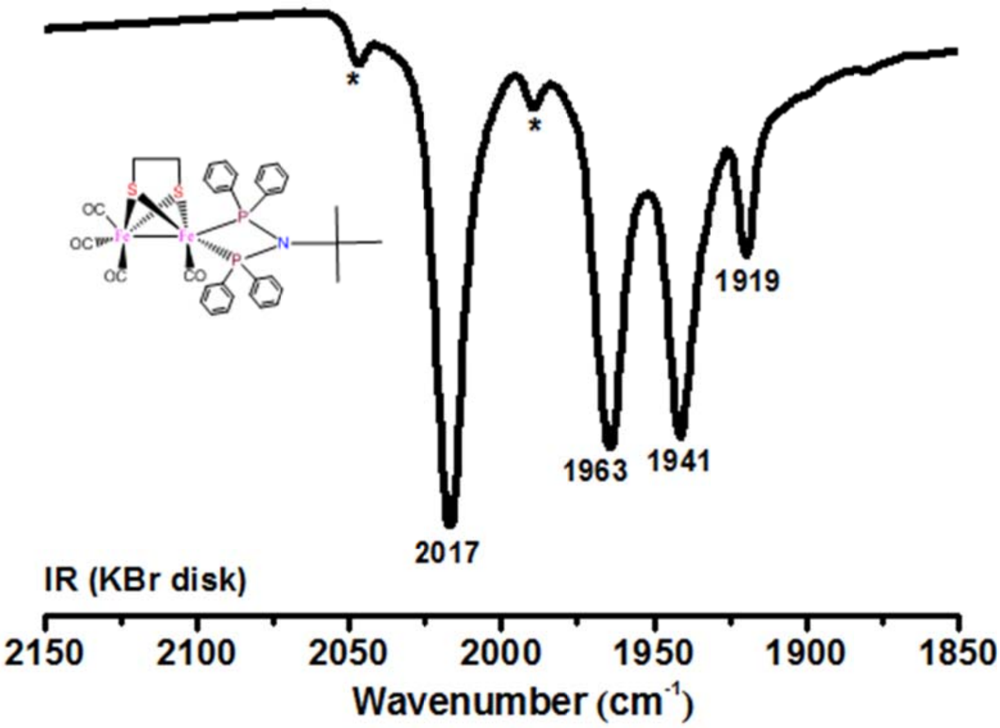

Figure S24(B). FT-IR spectrum of Fe_2(μ-edt)$(CO)_4${κ^2-$(Ph_2P)_2NCMe_3$} (**2a**) obtained from UV irradiation (method ii) in KBr disk. (*The two peaks might be assigned to a very small amount of byproduct [Fe_2(μ-edt)$(CO)_5${κ^1-$Ph_2P(NHBu^t)$}]).

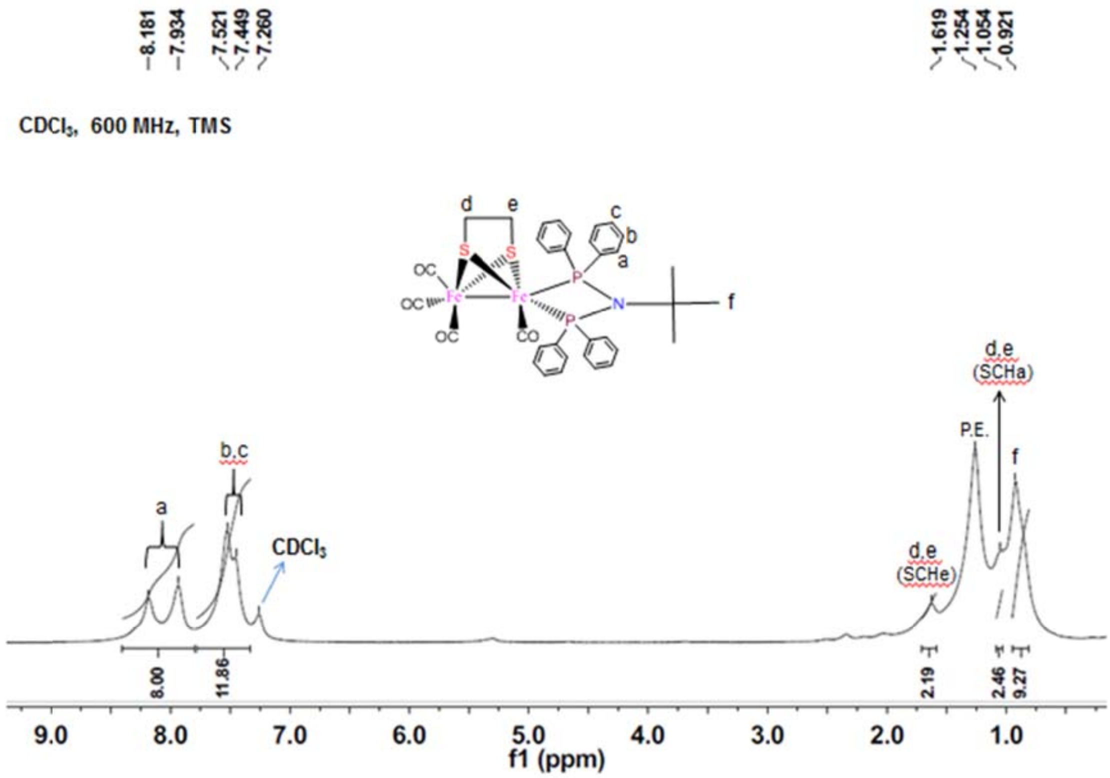

Figure S25. ^{1}H NMR spectrum of $Fe_2(\mu\text{-edt})(CO)_4\{\kappa^2\text{-}(Ph_2P)_2NCMe_3\}$ (**2a**) in $CDCl_3$.

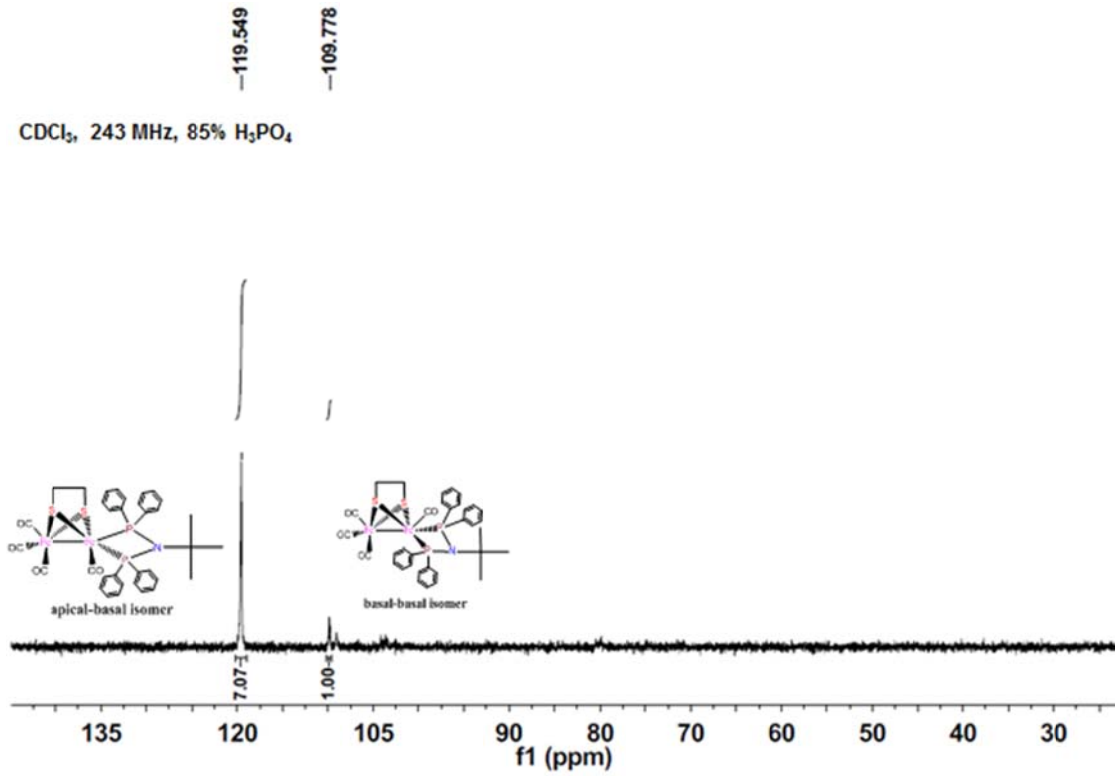

Figure S26. $^{31}P\{^{1}H\}$ NMR spectrum of $Fe_2(\mu\text{-edt})(CO)_4\{\kappa^2\text{-}(Ph_2P)_2NCMe_3\}$ (**2a**) in $CDCl_3$.

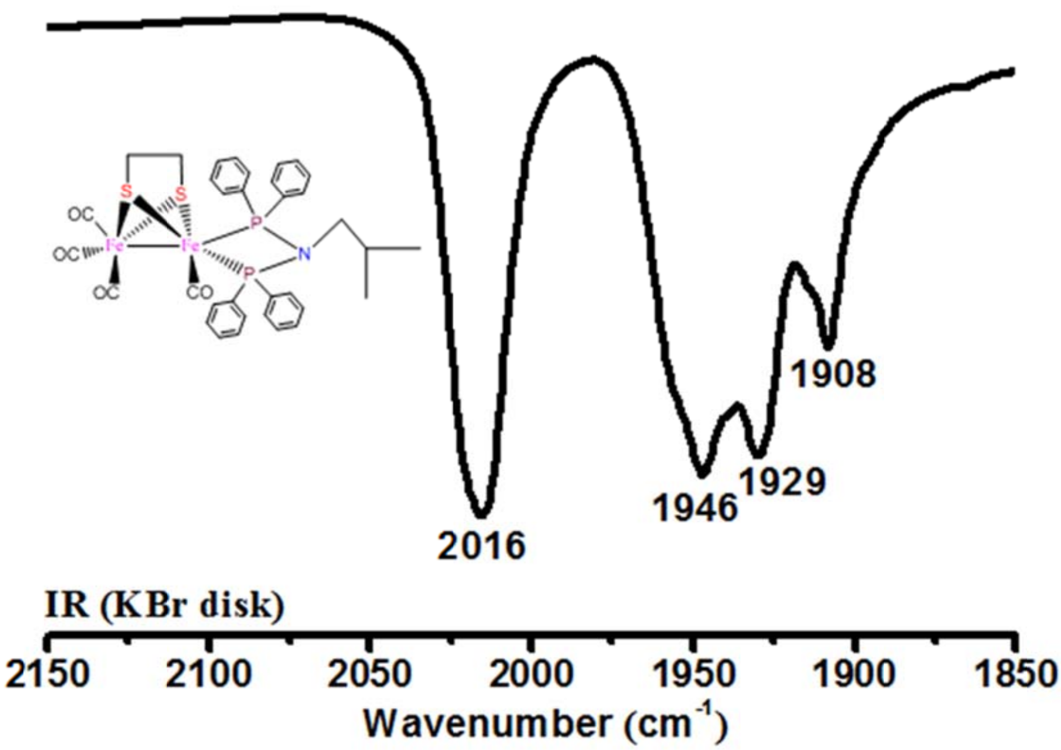

Figure S27(A). FT-IR spectrum of $Fe_2(\mu\text{-edt})(CO)_4\{\kappa^2\text{-}(Ph_2P)_2NCH_2CHMe_2\}$ (**2b**) obtained from oxidative decarbonylation (method i) in KBr disk.

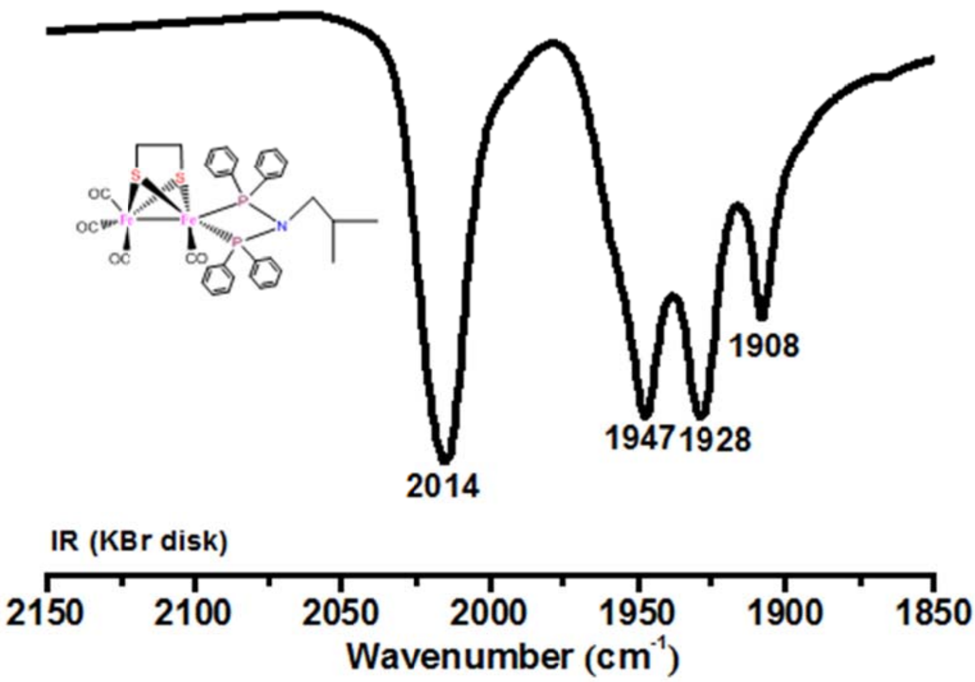

Figure S27(B). FT-IR spectrum of $Fe_2(\mu\text{-edt})(CO)_4\{\kappa^2\text{-}(Ph_2P)_2NCH_2CHMe_2\}$ (**2b**) obtained from UV irradiation (method ii) in KBr disk.

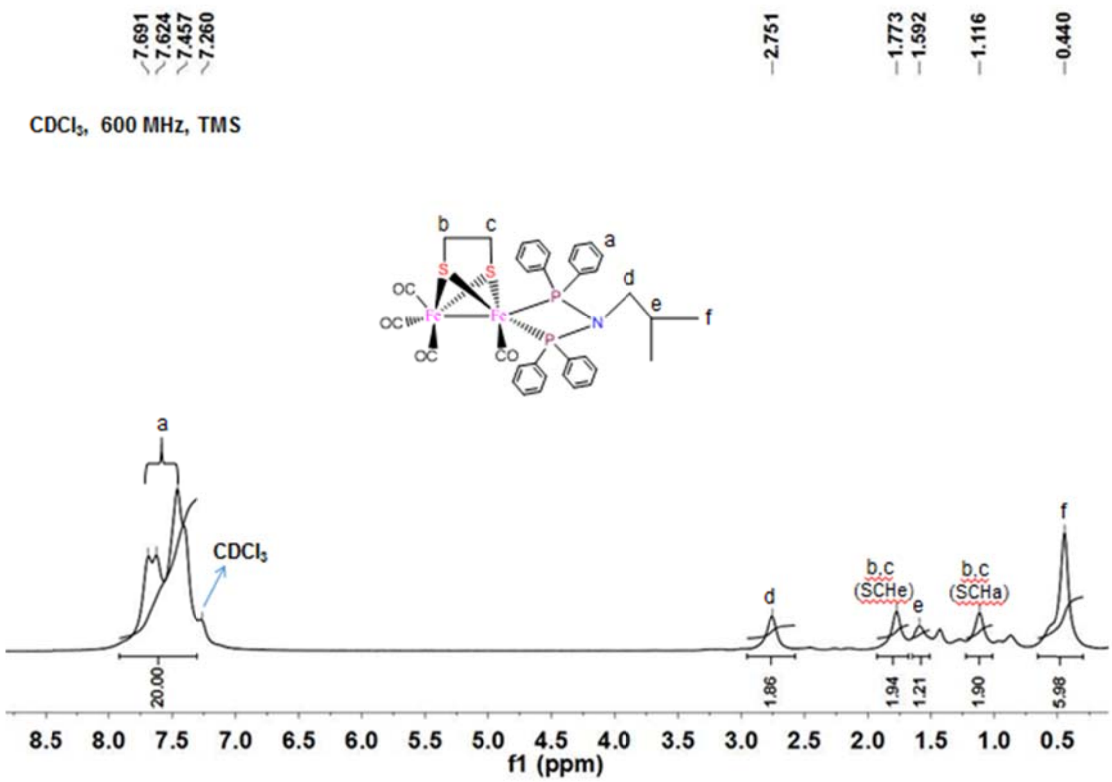

Figure S28. ^{1}H NMR spectrum of $Fe_2(\mu$-edt$)(CO)_4\{\kappa^2$-$(Ph_2P)_2NCH_2CHMe_2\}$ (**2b**) in $CDCl_3$.

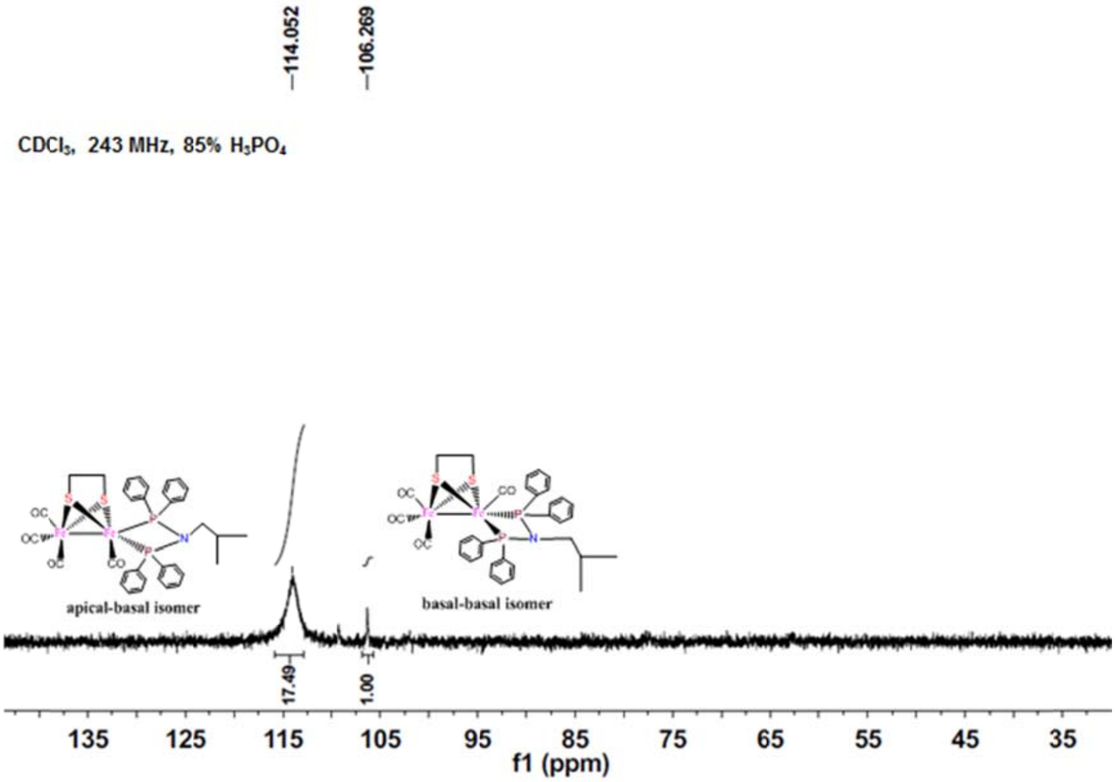

Figure S29. $^{31}P\{^1H\}$ NMR spectrum of $Fe_2(\mu\text{-edt})(CO)_4\{\kappa^2\text{-}(Ph_2P)_2NCH_2CHMe_2\}$ (**2b**) in $CDCl_3$.

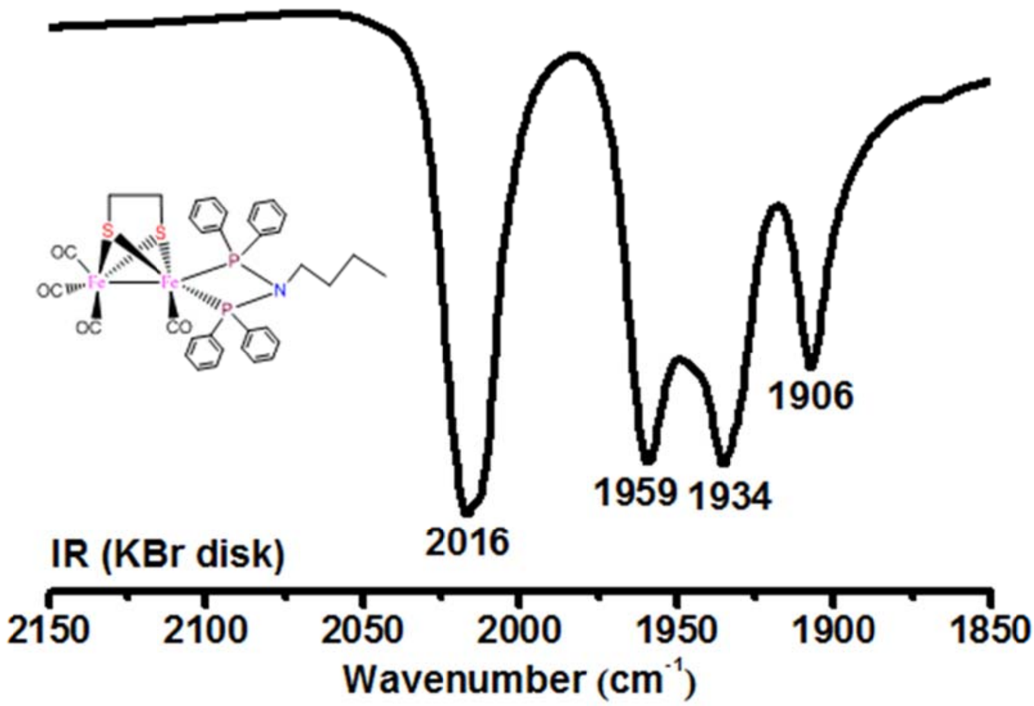

Figure S30(A). FT-IR spectrum of $Fe_2(\mu\text{-edt})(CO)_4\{\kappa^2\text{-}(Ph_2P)_2N(CH_2)_3Me\}$ (**2c**) obtained from oxidative decarbonylation (method i) in KBr disk.

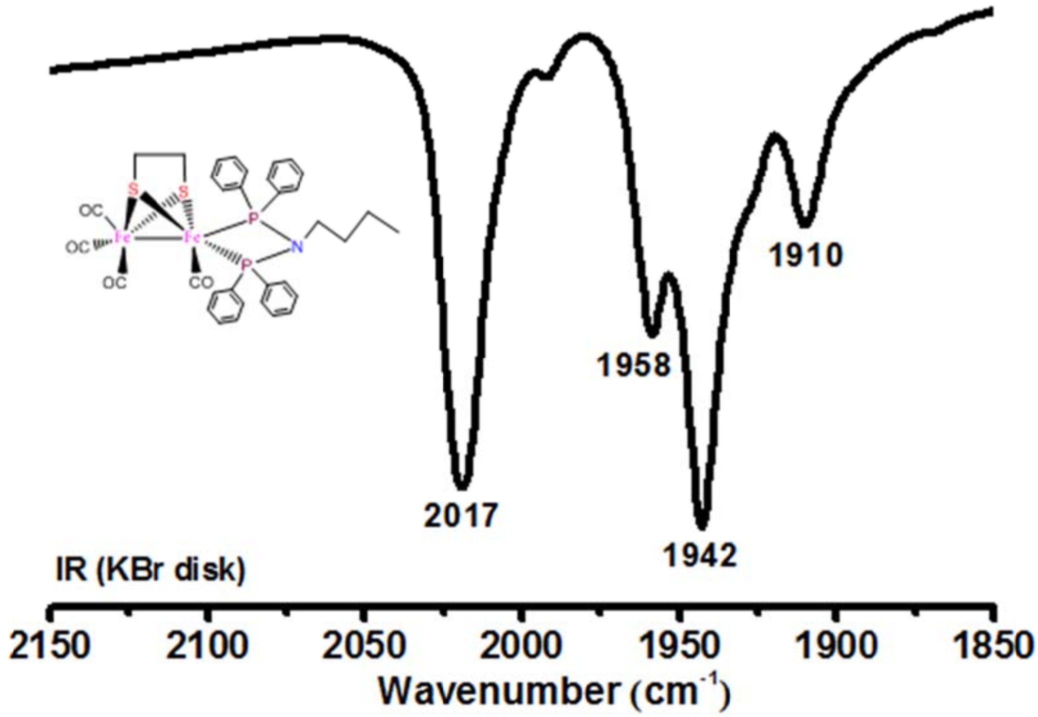

Figure S30(B). FT-IR spectrum of $Fe_2(\mu\text{-edt})(CO)_4\{\kappa^2\text{-}(Ph_2P)_2N(CH_2)_3Me\}$ (**2c**) obtained from UV irradiation (method ii) in KBr disk.

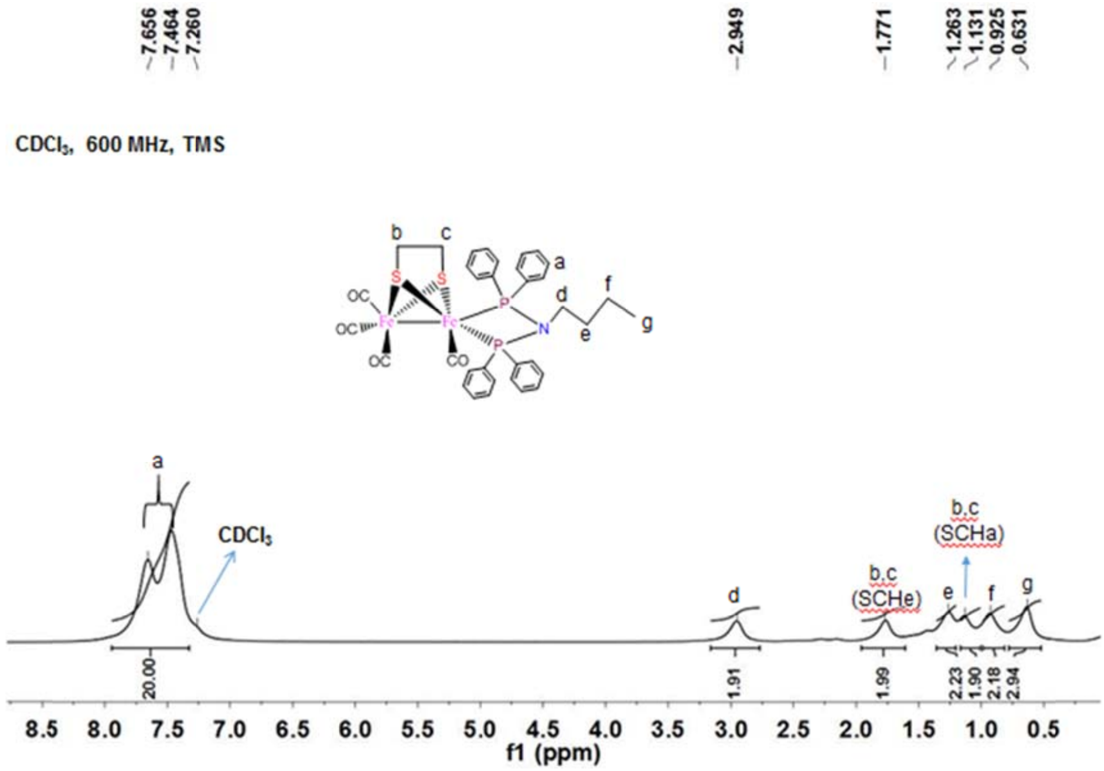

Figure S31. ^{1}H NMR spectrum of $Fe_2(\mu\text{-edt})(CO)_4\{\kappa^2\text{-}(Ph_2P)_2N(CH_2)_3Me\}$ (**2c**) in $CDCl_3$.

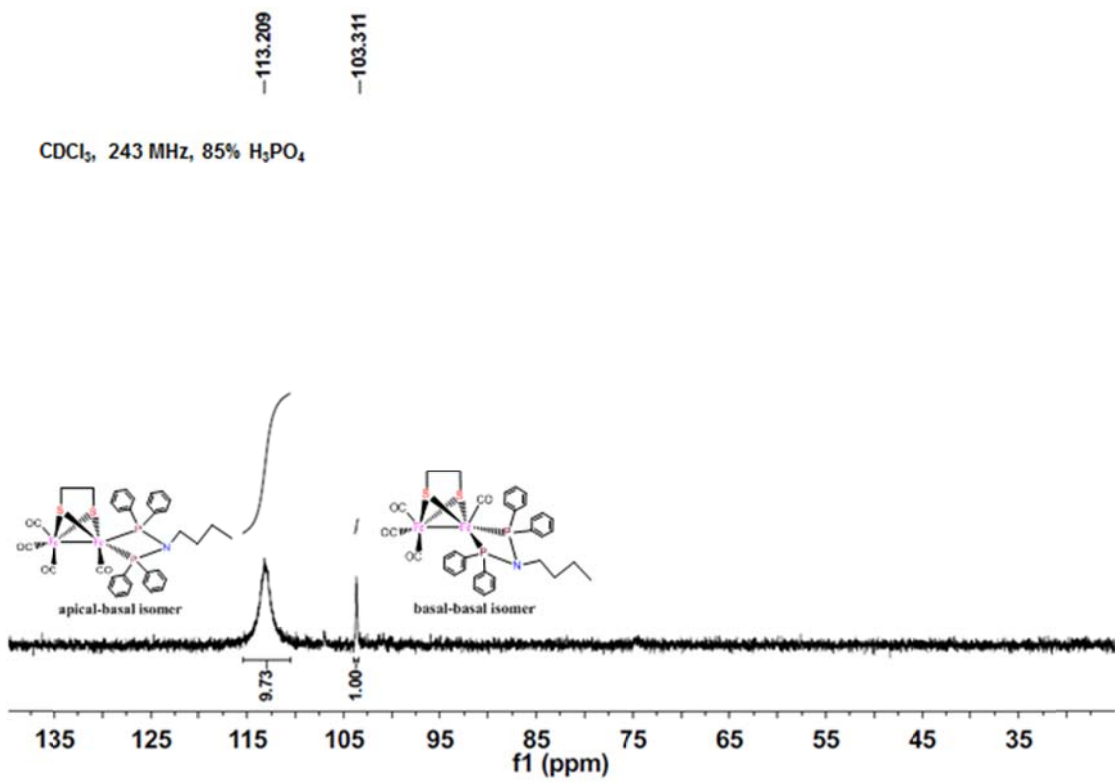

Figure S32. $^{31}P\{^{1}H\}$ NMR spectrum of $Fe_2(\mu\text{-edt})(CO)_4\{\kappa^2\text{-}(Ph_2P)_2N(CH_2)_3Me\}$ (**2c**) in $CDCl_3$.

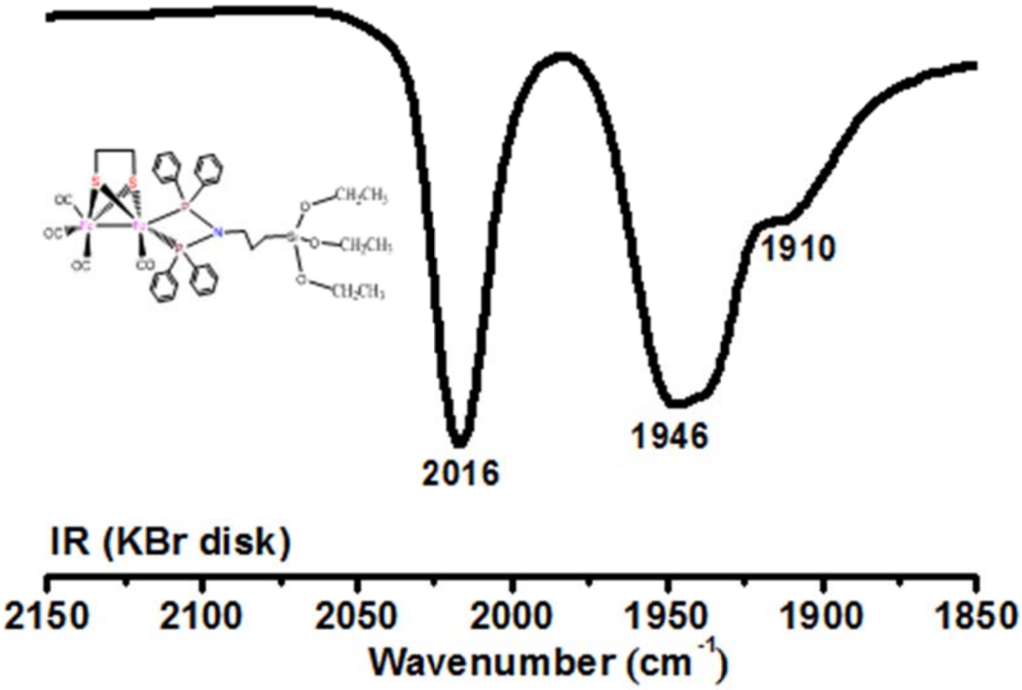

Figure S33(A). FT-IR spectrum of $Fe_2(\mu\text{-edt})(CO)_4\{\kappa^2\text{-}(Ph_2P)_2N(CH_2)_2Si(OEt)_3\}$ (**2d**) obtained from oxidative decarbonylation (method i) in KBr disk.

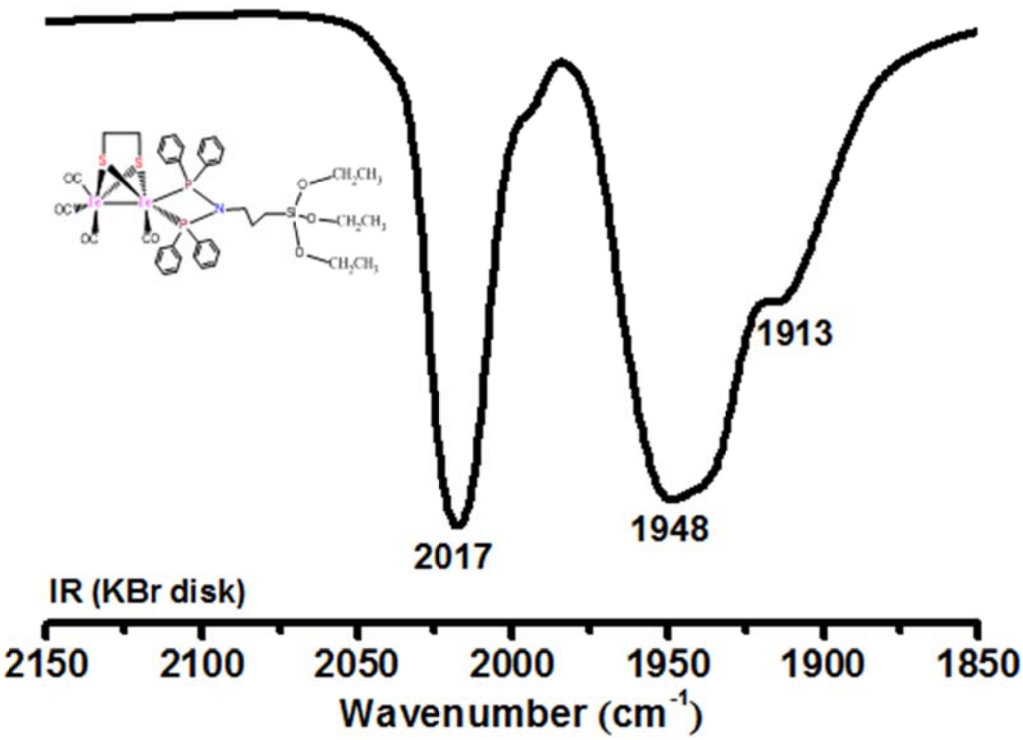

Figure S33(B). FT-IR spectrum of $Fe_2(\mu\text{-edt})(CO)_4\{\kappa^2\text{-}(Ph_2P)_2N(CH_2)_2Si(OEt)_3\}$ (**2d**) obtained from UV irradiation (method ii) in KBr disk.

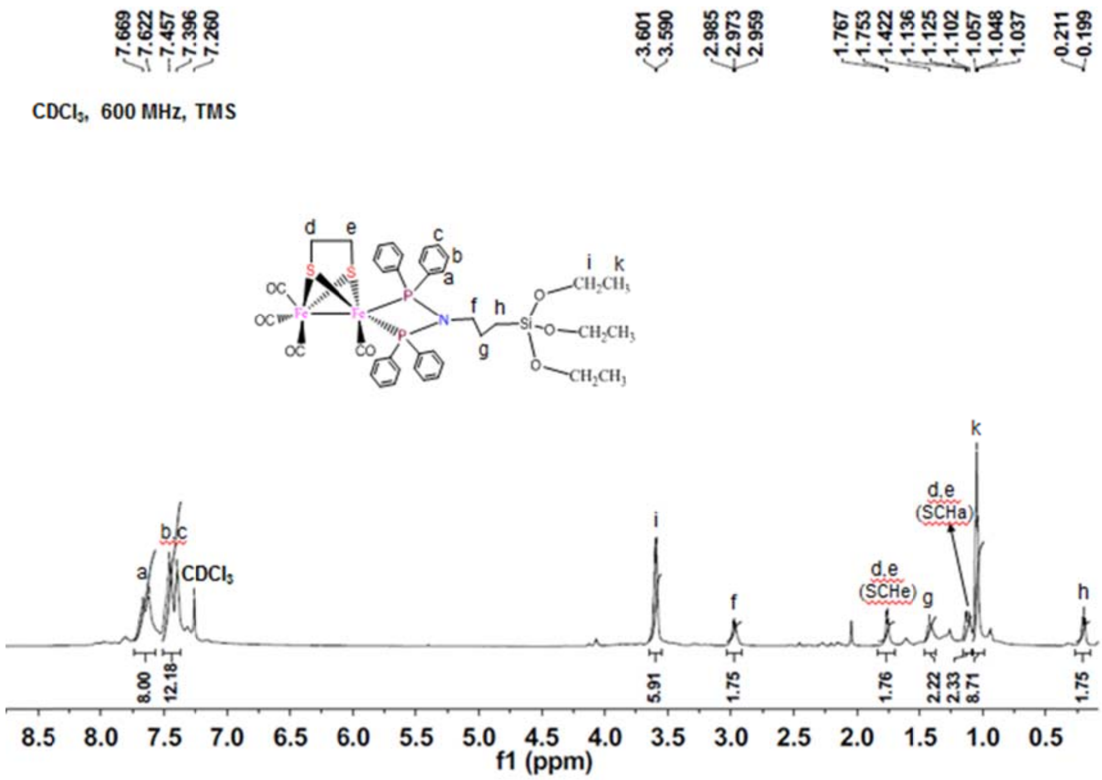

Figure S34. ^{1}H NMR spectrum of $Fe_2(\mu\text{-edt})(CO)_4\{\kappa^2\text{-}(Ph_2P)_2N(CH_2)_2Si(OEt)_3\}$ (**2d**) in $CDCl_3$.

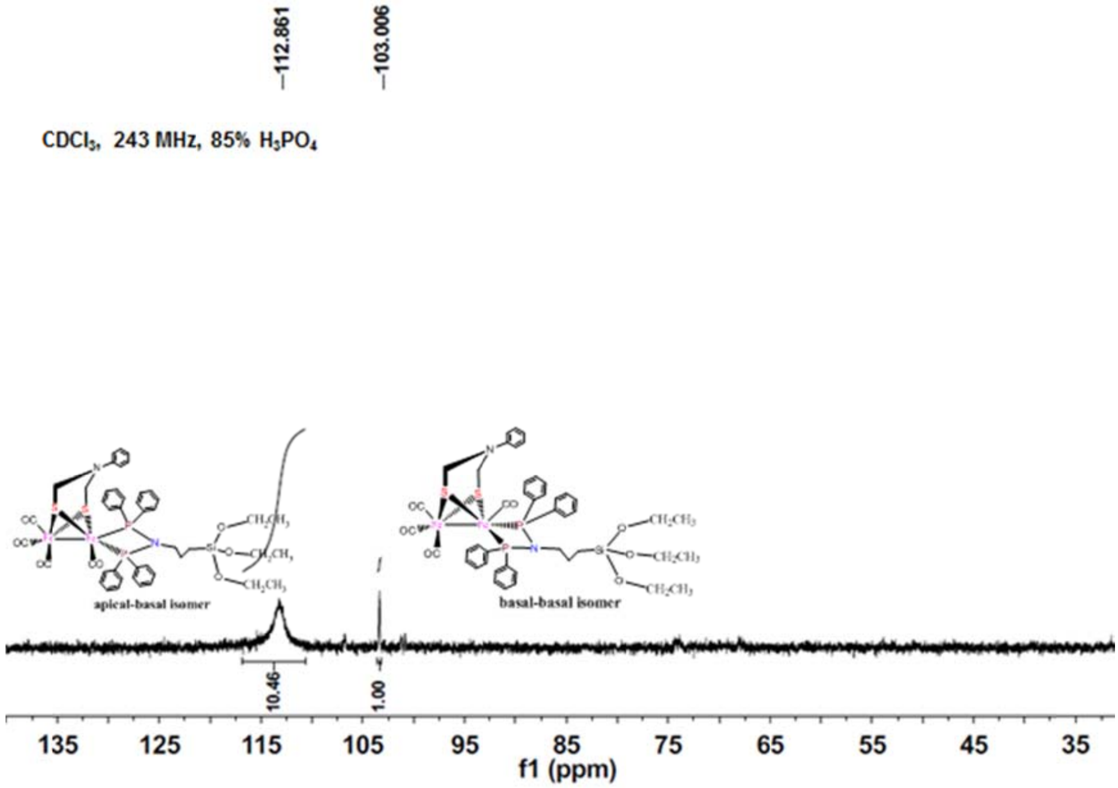

Figure S35. $^{31}P\{^1H\}$ NMR spectrum of $Fe_2(\mu\text{-edt})(CO)_4\{\kappa^2\text{-}(Ph_2P)_2N(CH_2)_2Si(OEt)_3\}$ (**2d**) in $CDCl_3$.

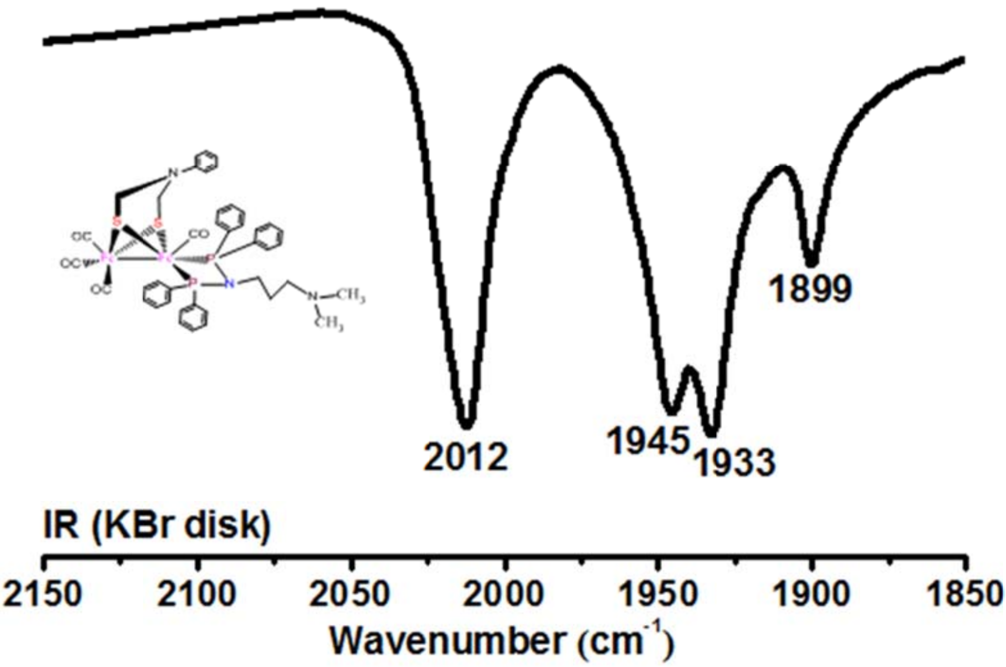

Figure S36(A). FT-IR spectrum of $Fe_2(\mu\text{-edt})(CO)_4\{\kappa^2\text{-}(Ph_2P)_2N(CH_2)_3NMe_2\}$ (**2e**) obtained from oxidative decarbonylation (method i) in KBr disk.

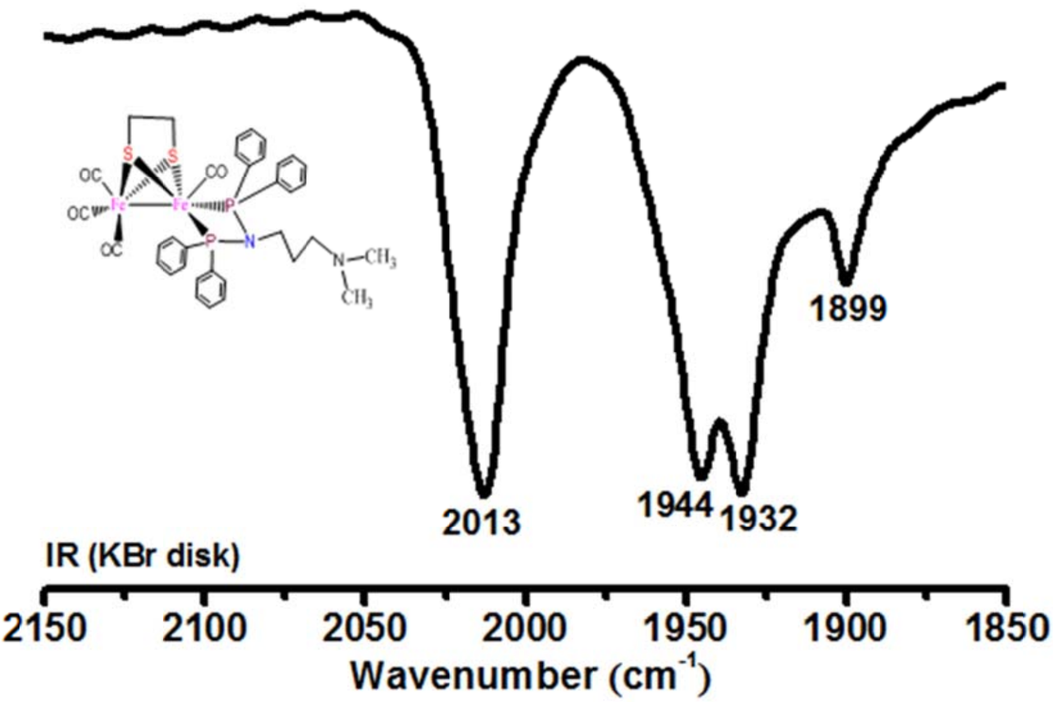

Figure S36(B). FT-IR spectrum of $Fe_2(\mu\text{-edt})(CO)_4\{\kappa^2\text{-}(Ph_2P)_2N(CH_2)_3NMe_2\}$ (**2e**) obtained from UV irradiation (method ii) in KBr disk.

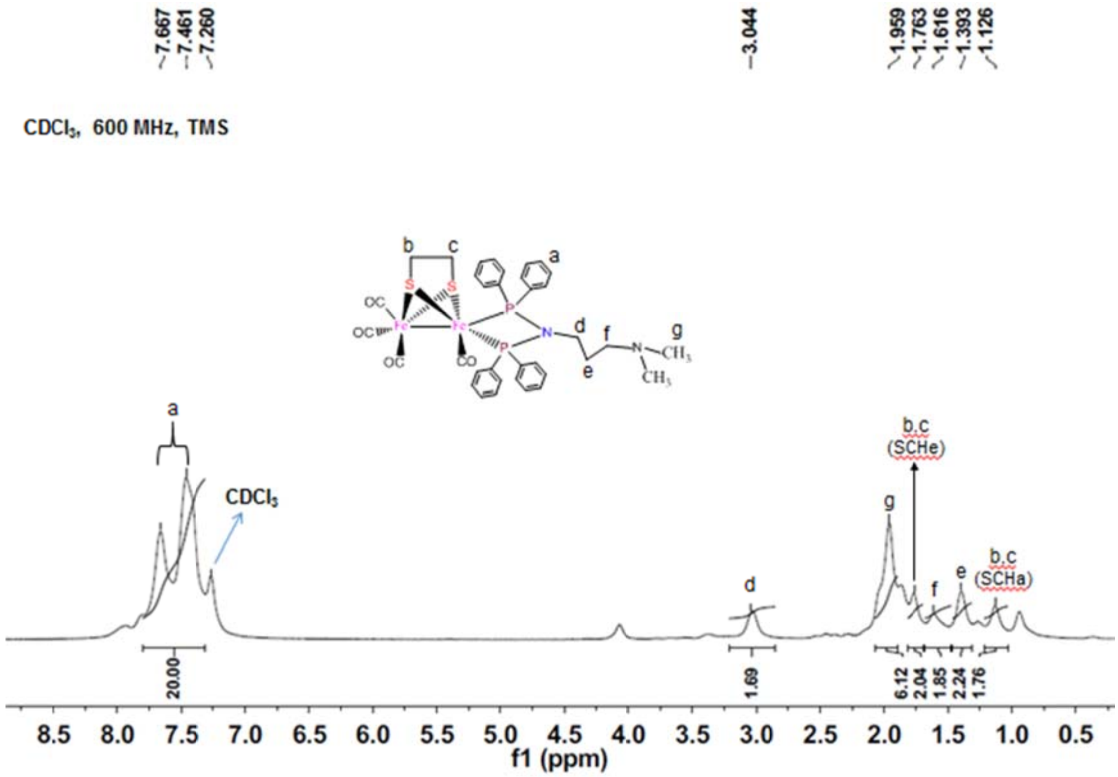

Figure S37. ^{1}H NMR spectrum of $Fe_2(\mu\text{-edt})(CO)_4\{\kappa^2\text{-}(Ph_2P)_2N(CH_2)_3NMe_2\}$ (**2e**) in $CDCl_3$.

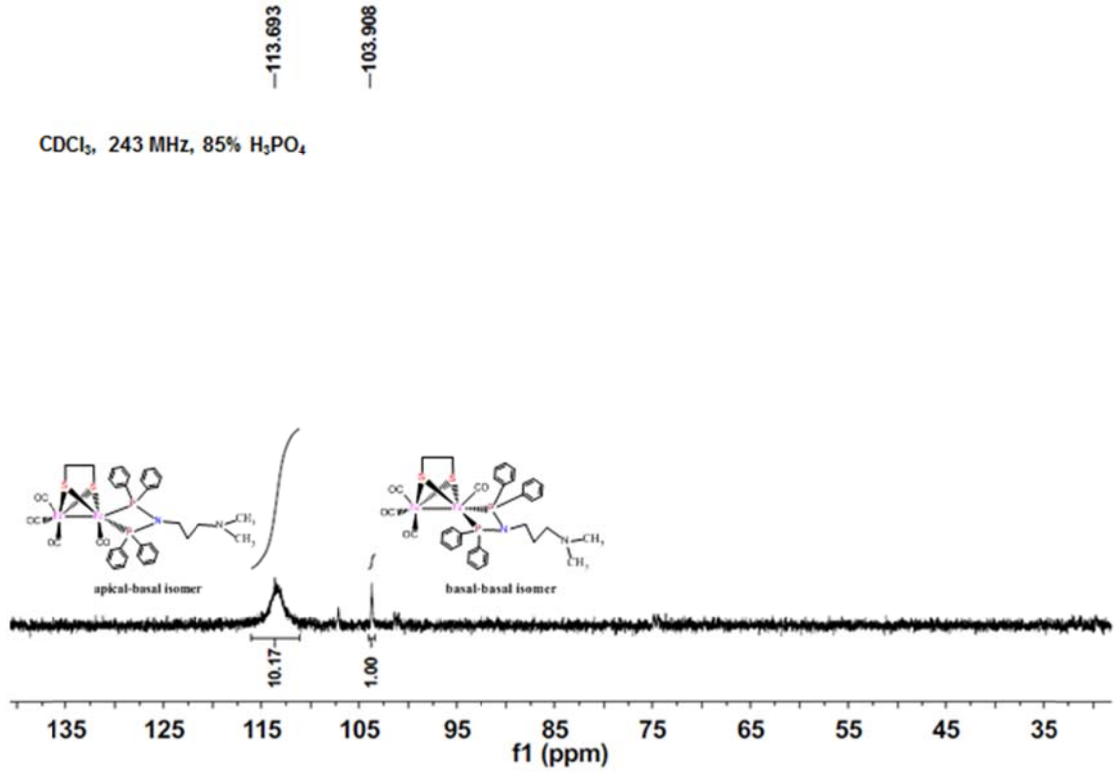

Figure S38. $^{31}P\{^{1}H\}$ NMR spectrum of $Fe_2(\mu\text{-edt})(CO)_4\{\kappa^2\text{-}(Ph_2P)_2N(CH_2)_3NMe_2\}$ (**2e**) in $CDCl_3$.